

# New approach to approximate analytical solutions of a harmonic oscillator with weak to moderate nonlinear damping: Part I

Karlo Lelas<sup>\*1, †</sup> and Robert Pezer<sup>2, ‡</sup>

<sup>1</sup>*Faculty of Textile Technology, University of Zagreb,  
Prilaz baruna Filipovića 28a, 10000 Zagreb, Croatia*

<sup>2</sup>*Department of Physical Metallurgy, Faculty of Metallurgy,  
University of Zagreb, Aleja narodnih heroja 3, 44000 Sisak, Croatia*

(Dated: December 30, 2025)

We introduce a new approach to deriving approximate analytical solutions of a harmonic oscillator damped by purely nonlinear, or combinations of linear and nonlinear damping forces. Our approach is based on choosing a suitable trial solution, i.e. an ansatz, which is the product of the time-dependent amplitude and the oscillatory (trigonometric) function that has the same frequency but different initial phase, compared to the undamped case. We derive the equation for the amplitude decay using the connection of the energy dissipation rate with the power of the total damping force and the approximation that the amplitude changes slowly over time compared to the oscillating part of the ansatz. By matching our ansatz to the initial conditions, we obtain the equations for the corresponding initial amplitude and initial phase. Here we demonstrate the validity of our approach in the case of damping quadratic in velocity, Coulomb damping, and a combination of the two, i.e. in this paper we consider purely nonlinear damping, while the dynamics with combinations of damping linear in velocity and nonlinear damping will be analyzed in a follow-up paper. In the case of damping quadratic in velocity, by comparing our approximate analytical solutions with the corresponding numerical solutions, we find that our solutions excellently describe the dynamics of the oscillator in the regime of weak to moderately strong quadratic damping. In the case of Coulomb damping, as well as in the case of a combined Coulomb and quadratic damping, our approximate analytical solutions agree well with the corresponding numerical solutions until the last few half-periods of the motion. Therefore, for these two cases, we introduce improved variants of our approximate solutions which describe the dynamics well until the very end. Furthermore, we show that our approximate solutions agree significantly better with the numerical ones than the solutions obtained by a known approach that uses a similar ansatz, but in which the initial phase remains the same as in the corresponding undamped solution.

## I. INTRODUCTION

In physics and engineering, the decrease in the amplitude of free harmonic oscillations is usually attributed to one of the three different types of damping: damping linear in velocity, damping quadratic in velocity, and sliding friction. In the case of a harmonic oscillator damped by a force linear in velocity (viscous damping), the corresponding equation of motion can be solved exactly and the solutions can be easily analyzed [1–4]. In case of a harmonic oscillator damped with sliding friction (Coulomb damping), the corresponding equation of motion is nonlinear because the friction force reverses direction with velocity, which is modeled via the signum function, but it can still be solved exactly by splitting the motion into left and right moving segments [5–8], i.e. the motion needs to be analyzed over half-periods and the solution thus obtained is piecewise continuous. In the case of a harmonic oscillator with damping quadratic in velocity, the corresponding equation of motion is a nonlinear differential equation that cannot be solved analytically and approximate or numerical methods must be used [7, 9–11]. Therefore, even for a harmonic oscillator with only one type of damping present, the analysis of the dynamics can be challenging if the damping is nonlinear, i.e. Coulomb damping or damping quadratic in velocity.

Although the damped harmonic oscillator model, with a single type of damping, can successfully describe some simple real-world systems, such as physical pendulums [11], block-spring systems [8], RLC circuits [12], etc., for a more complete and precise description, it is necessary to take into account that oscillations are damped simultaneously by two or all three types of damping. For example, in [13] a simple physical pendulum was studied, both experimentally and theoretically, and it was shown that the contribution of all three types of damping must be taken into account

---

<sup>\*</sup> Corresponding author

<sup>†</sup>Electronic address: [klelas@ttf.unizg.hr](mailto:klelas@ttf.unizg.hr)

<sup>‡</sup>Electronic address: [rpezer@simet.unizg.hr](mailto:rpezer@simet.unizg.hr)

for an adequate general description of pendulum damping, while in some specific cases two types of damping were sufficient.

In a recent paper [14], a harmonic oscillator damped simultaneously by all three types of damping was studied and approximate analytical solutions were found that agree excellently with numerical solutions, but only in the weak damping regime. The approach used in [14] is based on ansatz of the form  $\tilde{x}(t) = A_0 \tilde{f}(t) \cos(\omega_0 t + \varphi_0)$ , where  $\omega_0$ ,  $A_0$ , and  $\varphi_0$  are the angular frequency, amplitude, and initial phase of the corresponding undamped solution, while  $\tilde{f}(t)$  is the unknown function that describes the decay of the amplitude over time. The connection of the energy dissipation rate and the power of the total damping force was used to determine the unknown function  $\tilde{f}(t)$  [14]. More precisely, in the case of weak damping, one can take that  $\tilde{f}(t)$  remains approximately constant over half cycles (half periods) and average the oscillatory parts of the energy dissipation rate to obtain the first-order differential equation for  $\tilde{f}(t)$ . The same approach was previously used to determine the amplitude decay in the case of weak damping by each of the three types of damping individually [11], by combination of viscous damping and damping quadratic in velocity [15], and by combination of Coulomb damping and viscous damping [16]. The advantage of this approach is mathematical simplicity, but, of course, with the increase in the strength of the damping the values of angular frequency, initial phase, and (initial) amplitude can change significantly compared to the undamped case.

The analysis of the influence of the damping strength on the initial phase and frequency carried out in [17] for viscous damping and carried out in [14] for damping quadratic in velocity clearly shows that better approximate analytical solutions can be obtained already if we simply take that the initial phase and the initial amplitude of the approximate analytical solution differ from  $\varphi_0$  and  $A_0$ , but still keep  $\omega_0$  as its angular frequency. Thus, here we use an ansatz of the form  $x(t) = A f(t) \cos(\omega_0 t + \varphi)$  as the basis of our approach. In addition to the unknown function  $f(t)$ , we now have to determine the constants  $A$  and  $\varphi$ , i.e. we have a somewhat more complex mathematical problem compared to the approach used in [14], but, as we will show, we obtain new approximate analytical solutions that describe the dynamics significantly better and are valid for a wider range of values of the corresponding damping constants than the solutions obtained in [14].

This paper is organized into five sections. In Section II, we consider the case of harmonic oscillator damped simultaneously by all three types of damping, introduce the theory and approximations we use and derive the first-order differential equation for the amplitude decay, the equation for the initial amplitude, and the equation for the initial phase. In Section III, we obtain new approximate analytical solutions for damping quadratic in velocity. In Section IV, we obtain new approximate analytical solutions in the case of Coulomb damping. In Section V, we obtain new approximate analytical solutions for combined Coulomb and quadratic damping. In each of Sections III, IV, and V we compare new solutions to the corresponding solutions obtained by the approach used in [14] and numerical solutions. We note here for clarity that throughout the paper new solutions are designated with  $x(t)$ , corresponding energies with  $E(t)$ , and both are shown as solid red curves in all figures, solutions obtained by the approach used in [14] are designated with  $\tilde{x}(t)$ , corresponding energies with  $\tilde{E}(t)$ , and both are shown as solid blue curves in all figures, while numerical solutions and numerically obtained energies are shown as dotted black curves in all figures. At the end of each of Sections III, IV, and V we discuss the results for the type of damping considered. In Section VI, we summarize the important findings of the paper and provide an outlook for the follow-up paper that will cover the cases of combined linear and nonlinear damping.

## II. NEW EQUATIONS FOR THE AMPLITUDE DECAY, INITIAL AMPLITUDE, AND INITIAL PHASE

We consider the paradigmatic example of a damped harmonic oscillator shown in Fig. 1, i.e. a block of mass  $m$  that oscillates back and forth along a horizontal surface under the influence of the restoring force of an ideal spring  $F_{res}(t) = -kx(t)$ , where  $k$  is the stiffness of the spring and  $x(t)$  is the displacement of the block from the equilibrium position (set to  $x = 0$ ), and under the influence of the damping force

$$F_d(t) = -\text{sgn}[v(t)]\mu mg - bv(t) - Dv(t)|v(t)|, \quad (1)$$

where  $\mu > 0$ ,  $b > 0$  and  $D > 0$  are the corresponding damping constants,  $v(t) = dx(t)/dt$  is the velocity, and

$$\text{sgn}[v(t)] = \begin{cases} 1 & \text{if } v(t) > 0 \\ 0 & \text{if } v(t) = 0 \\ -1 & \text{if } v(t) < 0 \end{cases} \quad (2)$$

is the sign function. The corresponding equation of motion is

$$ma(t) = -\text{sgn}[v(t)]\mu mg - bv(t) - Dv(t)|v(t)| - kx(t), \quad (3)$$

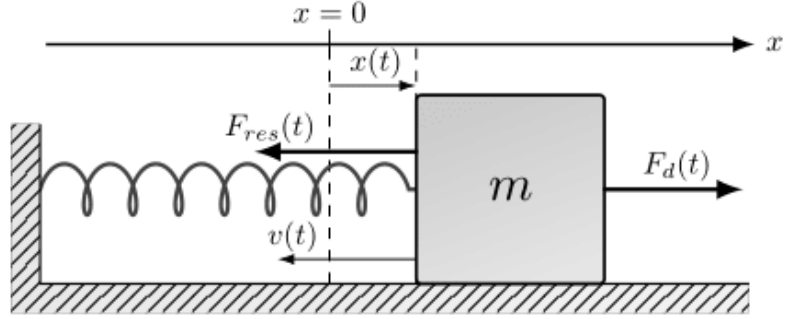


FIG. 1: Schematic representation of a block-spring system with a restoring force  $F_{res}(t)$  and a (total) damping force  $F_d(t)$ . Here we show the time instant at which  $x(t) > 0$  and  $v(t) < 0$ , i.e. at which  $F_{res}(t) < 0$  and  $F_d(t) > 0$ . See text for details.

where  $a(t) = d^2x(t)/dt^2$  is the acceleration of the block. The first term on the right-hand side of equation (3) models the force of sliding friction [5–7, 18, 19], while the second and third terms model, e.g., the influence of air resistance, since air resistance generally depends on terms proportional to velocity and square of velocity [11, 13, 15, 20]. For simplicity, here we assume that the static and dynamic coefficients of friction are the same, i.e. both are equal to  $\mu$ . The energy (potential plus kinetic) of the block-spring system is given by

$$E(t) = \frac{kx^2(t)}{2} + \frac{mv^2(t)}{2}. \quad (4)$$

If we put  $\mu = b = D = 0$  in (3), i.e. for  $F_d(t) = 0$ , we get the equation of the undamped harmonic oscillator [3], with general solution

$$x_{HO}(t) = A_0 \cos(\omega_0 t + \varphi_0), \quad (5)$$

where  $\omega_0 = \sqrt{k/m}$  is the angular frequency of the undamped system, while  $A_0$  and  $\varphi_0$  are constants (amplitude and initial phase) that are determined from initial conditions  $(x_0, v_0)$ , i.e.

$$A_0 = \sqrt{x_0^2 + \left(\frac{v_0}{\omega_0}\right)^2}, \quad \varphi_0 = \arctan\left(-\frac{v_0}{\omega_0 x_0}\right). \quad (6)$$

The undamped system oscillates with conserved, i.e. constant, energy [3]. For damped systems, i.e. for  $F_d(t) \neq 0$ , the energy is not conserved due to the power of the damping force  $P_d(t) = F_d(t)v(t)$ , and the energy dissipation rate is given by  $dE(t)/dt = P_d(t)$ , i.e.

$$\frac{dE(t)}{dt} = -\mu mg|v(t)| - bv^2(t) - D|v(t)|^3, \quad (7)$$

where we used  $\text{sgn}[v(t)]v(t) = |v(t)|$  and  $v^2(t)|v(t)| = |v(t)|^3$ . Thus, equation (7) tells us that the energy of the damped system decreases monotonically with time, i.e.  $\frac{dE(t)}{dt} \leq 0$  for all  $t \geq 0$ , and  $\frac{dE(t)}{dt} = 0$  holds at the turning points, i.e. at instants when  $v(t) = 0$ .

In a recent paper [14], approximate analytical solutions of harmonic oscillator weakly damped by a force (1) were derived starting from the simple ansatz

$$\tilde{x}(t) = A_0 \tilde{f}(t) \cos(\omega_0 t + \varphi_0), \quad (8)$$

where  $A_0$ ,  $\omega_0$  and  $\varphi_0$  are the same as in the undamped case, i.e. as in (5), while the unknown function  $\tilde{f}(t)$  describes the slow decay of oscillations with time. By slow decay we mean that the rate of change of the function  $\tilde{f}(t)$  over time is significantly slower than the rate of change of the function  $\cos(\omega_0 t + \varphi_0)$ . The approach in [14] is further based on taking

$$\tilde{v}(t) = -\omega_0 A_0 \tilde{f}(t) \sin(\omega_0 t + \varphi_0), \quad (9)$$

for velocity, i.e. in neglecting the term with  $d\tilde{f}(t)/dt$  in  $d\tilde{x}(t)/dt$ , which leads to energy of the form

$$\tilde{E}(t) = \frac{m\omega_0^2 A_0^2 \tilde{f}^2(t)}{2}. \quad (10)$$

These steps are justified in the case of weak damping, i.e. when the frequency and initial phase remain approximately the same as in the undamped case and  $|d\tilde{f}(t)/dt|\omega_0^{-1} \ll 1$  holds for all  $t \geq 0$  [14]. Simple first order differential equation for the function  $\tilde{f}(t)$  is obtained by inserting velocity (9) and energy (10) into the energy dissipation rate (7) and taking the time average of trigonometric functions over half periods [14]. It was shown (for a particular choice of  $m$ ,  $k$  and  $A_0$ ) that the approximate analytical solutions obtained by this approach are in excellent agreement with the numerical solutions for a certain limited range of values of the damping constants ( $\mu$ ,  $b$  and  $D$ ) and that this agreement also depends on the type of initial conditions considered (i.e. on  $\varphi_0$ ) [14]. In particular, the agreement of approximate analytical solutions of the form (8) with numerical solutions is better in the case of initial conditions ( $x_0 = 0, v_0 \neq 0$ ) with purely kinetic initial energy than in the case of initial conditions ( $x_0 \neq 0, v_0 = 0$ ) with purely potential initial energy [14].

Here we improve the approach used in [14] by starting from the ansatz of the form

$$x(t) = Af(t) \cos(\omega_0 t + \varphi), \quad (11)$$

where  $A \neq A_0$  and  $\varphi \neq \varphi_0$  are unknown constants and  $f(t)$  is the unknown function that describes the amplitude decay over time. The corresponding velocity is

$$v(t) = \frac{dx(t)}{dt} = -\omega_0 Af(t) \sin(\omega_0 t + \varphi) + A \frac{df(t)}{dt} \cos(\omega_0 t + \varphi). \quad (12)$$

Although we have not yet determined the function  $f(t)$ , without loss of generality, we can take  $f(0) = 1$ , and using initial conditions ( $x(0) = x_0, v(0) = v_0$ ) we obtain equations

$$x_0 = A \cos(\varphi) \quad (13)$$

and

$$v_0 = -\omega_0 A \sin(\varphi) + A \frac{df(t)}{dt} \bigg|_{t=0} \cos(\varphi) \quad (14)$$

from which we will determine the constants  $A$  and  $\varphi$  once we determine  $df(t)/dt$  at  $t = 0$ . The energy corresponding to (11) and (12) is

$$E(t) = \frac{m\omega_0^2 A^2}{2} \left( f^2(t) - f(t) \frac{df(t)}{dt} \omega_0^{-1} \sin(2\omega_0 t + 2\varphi) + \left( \frac{df(t)}{dt} \right)^2 \omega_0^{-2} \cos^2(\omega_0 t + \varphi) \right) \quad (15)$$

We note here that keeping the terms of order  $(df(t)/dt)\omega_0^{-1}$  and  $(df(t)/dt)^2\omega_0^{-2}$  in velocity (12) and energy (15) is necessary in modeling the influence of damping on  $A$  and  $\varphi$  and also to ensure that our modeled displacement (11), velocity (12), and energy (15) can be matched to the initial conditions, but in modeling the function  $f(t)$  itself the simplest way is to proceed similarly as in [14], i.e. we approximate the left hand side of the energy dissipation rate (7) by

$$\frac{dE(t)}{dt} \approx \frac{d}{dt} \left( \frac{m\omega_0^2 A^2 f^2(t)}{2} \right) = m\omega_0^2 A^2 f(t) \frac{df(t)}{dt} \quad (16)$$

and for the velocity appearing on the right hand side of (7) we use

$$v(t) \approx -\omega_0 Af(t) \sin(\omega_0 t + \varphi). \quad (17)$$

Thus, using (16) and (17) in (7) we get

$$\frac{df(t)}{dt} = -\frac{\mu g}{\omega_0 A} |\sin(\omega_0 t + \varphi)| - \frac{b}{m} f(t) \sin^2(\omega_0 t + \varphi) - \frac{D\omega_0 A}{m} f^2(t) |\sin(\omega_0 t + \varphi)|^3. \quad (18)$$

Since, by the assumption of weak damping, the rate of change of  $f(t)$  is significantly slower than the rate of change of trigonometric functions over time intervals of the order  $\Delta T = T_0 = 2\pi/\omega_0$ , we can make an additional approximation in equation (18) by averaging the trigonometric functions over time intervals  $\Delta T/2$ , i.e.

$$\frac{df(t)}{dt} = -\frac{\mu g}{\omega_0 A} \langle |\sin(\omega_0 t + \varphi)| \rangle - \frac{b}{m} f(t) \langle \sin^2(\omega_0 t + \varphi) \rangle - \frac{D\omega_0 A}{m} f^2(t) \langle |\sin(\omega_0 t + \varphi)|^3 \rangle, \quad (19)$$

where we use the notation  $\langle F(t) \rangle = (T_0/2)^{-1} \int_t^{t+T_0/2} F(t') dt'$ . Since  $\langle |\sin(\omega_0 t + \varphi)| \rangle = 2/\pi$ ,  $\langle \sin^2(\omega_0 t + \varphi) \rangle = 1/2$ , and  $\langle |\sin(\omega_0 t + \varphi)|^3 \rangle = 4/(3\pi)$  we get

$$\frac{df(t)}{dt} = - \left( d_2 A f^2(t) + d_1 f(t) + \frac{d_0}{A} \right), \quad (20)$$

where

$$d_0 = \frac{2\mu g}{\pi\omega_0}, \quad d_1 = \frac{b}{2m}, \quad d_2 = \frac{4D\omega_0}{3\pi m}, \quad (21)$$

as the final differential equation for the function  $f(t)$ . We are now in a position to write the final equations from which we determine the constants  $A$  and  $\varphi$ . Combining (13) and (14), along with (20), we get

$$v_0 + \left( d_2 A + d_1 + \frac{d_0}{A} \right) x_0 = -\omega_0 \sqrt{A^2 - x_0^2} \quad (22)$$

as the equation from which we determine  $A$ , and

$$\varphi = \arctan \left( -\frac{v_0 + (d_2 A + d_1 + \frac{d_0}{A}) x_0}{\omega_0 x_0} \right) \quad (23)$$

as the equation from which we can calculate the initial phase (once we determined  $A$  from (22)). The first order differential equation (20) can be solved by separation of variables and integration, i.e. we have to solve

$$\int_{f(0)}^{f(t)} \left( d_2 A f^2(t') + d_1 f(t') + \frac{d_0}{A} \right)^{-1} df(t') = - \int_0^t dt'. \quad (24)$$

Thus,  $f(t)$  in our ansatz (11) is obtained by solving (24). We note here that  $\tilde{f}(t)$  that appears in ansatz (8) is obtained by solving the integral of the same form as (24), but in which  $A_0$  is in place of  $A$  [14]. Thus, once  $f(t)$  is obtained, one easily obtains the corresponding  $\tilde{f}(t)$  by replacing  $A$  in  $f(t)$  with  $A_0$ . Furthermore, for initial conditions ( $x_0 = 0, v_0 > 0$ ) equation (22) gives  $A = A_0 = v_0/\omega_0$  and (23) gives  $\varphi = \varphi_0 = -\pi/2$ , i.e. the same values as in the undamped case. Thus, for this particular type of initial conditions, approximate analytical solutions (8) and (11) are the same, but the corresponding velocities (9) and (12), as well as the energies (10) and (15), are not the same.

For an easier comparison of approximate analytical solutions obtained by the new approach presented here with the solutions obtained by the approach used in [14], we will consider a block-spring system with the same parameters as in [14], i.e. we consider a block of mass  $m = 1\text{ kg}$  attached to a spring of stiffness  $k = 30\text{ N/m}$ , and we use  $g = 9.81\text{ m/s}^2$ . The corresponding undamped angular frequency is  $\omega_0 = 5.48\text{ s}^{-1}$  and the period of the undamped system is  $T_0 = 1.15\text{ s}$ . These values are along the lines of experiments performed on block-spring systems, e.g. see [8]. Throughout the paper, as in [14], we consider initial conditions that correspond to undamped solutions with  $A_0 = 0.2\text{ m}$  and various values of  $\varphi_0$ , e.g., for ( $x_0 = A_0, v_0 = 0$ ) we have  $\varphi_0 = 0$ , for ( $x_0 = 0, v_0 = \omega_0 A_0$ ) we have  $\varphi_0 = -\pi/2$ , etc.

For this choice of the parameters of block-spring system and initial conditions, solutions of the form (8), obtained in [14], describe well the dynamics governed by the equation (3) for a range of values of the damping constants  $\mu, b$  and  $D$  that correspond to

$$0 < \frac{d_0}{A_0} \lesssim 0.03\omega_0, \quad 0 < d_1 \lesssim 0.1\omega_0, \quad 0 < d_2 A_0 \lesssim 0.1\omega_0. \quad (25)$$

Values of  $d_0/A_0$ ,  $d_1$ , and  $d_2 A_0$  are suitable to quantify the damping strength, since the weak damping limit can be characterized by the relations  $d_0/A_0 \ll \omega_0$ ,  $d_1 \ll \omega_0$ , and  $d_2 A_0 \ll \omega_0$  [14]. In what follows, we will compare the approximate analytical solutions of the form (11) with the solutions of the form (8) and with the corresponding numerical solutions for various values of  $\mu, b$  and  $D$  such that  $d_0/A_0 \geq 0.03\omega_0$ ,  $d_1 \geq 0.1\omega_0$  and  $d_2 A_0 \geq 0.1\omega_0$  hold.

Our main goal is to obtain approximate analytical solutions of the equation of motion (3) (with all three types of damping present) that are more accurate than the solutions recently presented in [14], but since the approach that includes the determination of constants  $A$  and  $\varphi$  using equations (22) and (23) has not yet been investigated in the cases where only one type of nonlinear damping is present, e.g. for harmonic oscillator damped only by a force quadratic in velocity or only by sliding friction, we will first focus on those simpler cases.

### III. DAMPING QUADRATIC IN VELOCITY

If  $D > 0$  and  $\mu = b = 0$  (i.e.  $d_2 > 0$  and  $d_0 = d_1 = 0$ ), equation (22) becomes a quadratic equation in  $A$  and we easily get

$$A = \frac{2x_0v_0d_2 + \sqrt{4x_0^2v_0^2d_2^2 + 4(\omega_0^2 - x_0^2d_2^2)(v_0^2 + \omega_0^2x_0^2)}}{2(\omega_0^2 - x_0^2d_2^2)}, \quad (26)$$

while equation (23) simplifies to

$$\varphi = \arctan\left(-\frac{v_0 + x_0d_2A}{\omega_0x_0}\right). \quad (27)$$

In this case, solving the integral (24) gives

$$f(t) = \frac{1}{1 + d_2At}. \quad (28)$$

Thus, in case of damping quadratic in velocity, our approximate solution (11) becomes

$$x(t) = \left(\frac{A}{1 + d_2At}\right) \cos(\omega_0t + \varphi), \quad (29)$$

where  $A$  and  $\varphi$  are given by (26) and (27). In this case, the approach used in [14] gives

$$\tilde{x}(t) = \left(\frac{A_0}{1 + d_2A_0t}\right) \cos(\omega_0t + \varphi_0), \quad (30)$$

where  $A_0$  and  $\varphi_0$  are defined in (6).

#### A. Initial conditions ( $x_0 > 0, v_0 = 0$ )

For this type of initial conditions (26) and (27) reduce to

$$A = \frac{x_0}{\sqrt{1 - (d_2x_0/\omega_0)^2}} \text{ and } \varphi = \arctan\left(-\frac{d_2A}{\omega_0}\right), \quad (31)$$

while  $A_0 = x_0$  and  $\varphi_0 = 0$ . As noted earlier, throughout the paper we always choose the initial conditions that correspond to  $A_0 = 0.2m$ , i.e. we take here  $x_0 = 0.2m$ . In Fig. 2(a)-(d) we show solutions  $x(t)$  given by (29), solutions  $\tilde{x}(t)$  given by (30) and the corresponding numerical solutions for  $D/(kg/m) = \{1.18, 2.95, 5.89, 8.84\}$ , i.e. for  $d_2A_0/\omega_0 = \{0.1, 0.25, 0.5, 0.75\}$ , with initial conditions ( $x_0 = 0.2m, v_0 = 0$ ). The *ode45* MATLAB function has been utilized to obtain the corresponding numerical solutions of the equation (3). We can see that the solutions  $x(t)$  agree better with the numerical results than the solutions  $\tilde{x}(t)$  for all chosen values of the ratio  $d_2A_0/\omega_0$ . In Fig. 2(a) we have shown a shorter time span compared to Fig. 2(b)-(d), in order to make the difference between  $x(t)$  and  $\tilde{x}(t)$  more visible.

In Fig. 3(a)-(d) we show the energies  $E(t)$  given by (15), the energies  $\tilde{E}(t)$  given by (10), and the corresponding numerically obtained energies for  $d_2A_0/\omega_0 = \{0.1, 0.25, 0.5, 0.75\}$  with initial conditions ( $x_0 = 0.2m, v_0 = 0$ ). For the chosen parameters of the block-spring system and the chosen values of the initial conditions, we have  $E(0) = \tilde{E}(0) = 0.6 J$ .

#### B. Initial conditions ( $x_0 = 0, v_0 > 0$ )

For this type of initial conditions, (26) and (27) simplify to  $A = A_0 = v_0/\omega_0$  and  $\varphi = \varphi_0 = -\pi/2$ , i.e. (29) and (30) become

$$x(t) = \tilde{x}(t) = \frac{v_0}{\omega_0(1 + d_2v_0t/\omega_0)} \sin(\omega_0t). \quad (32)$$

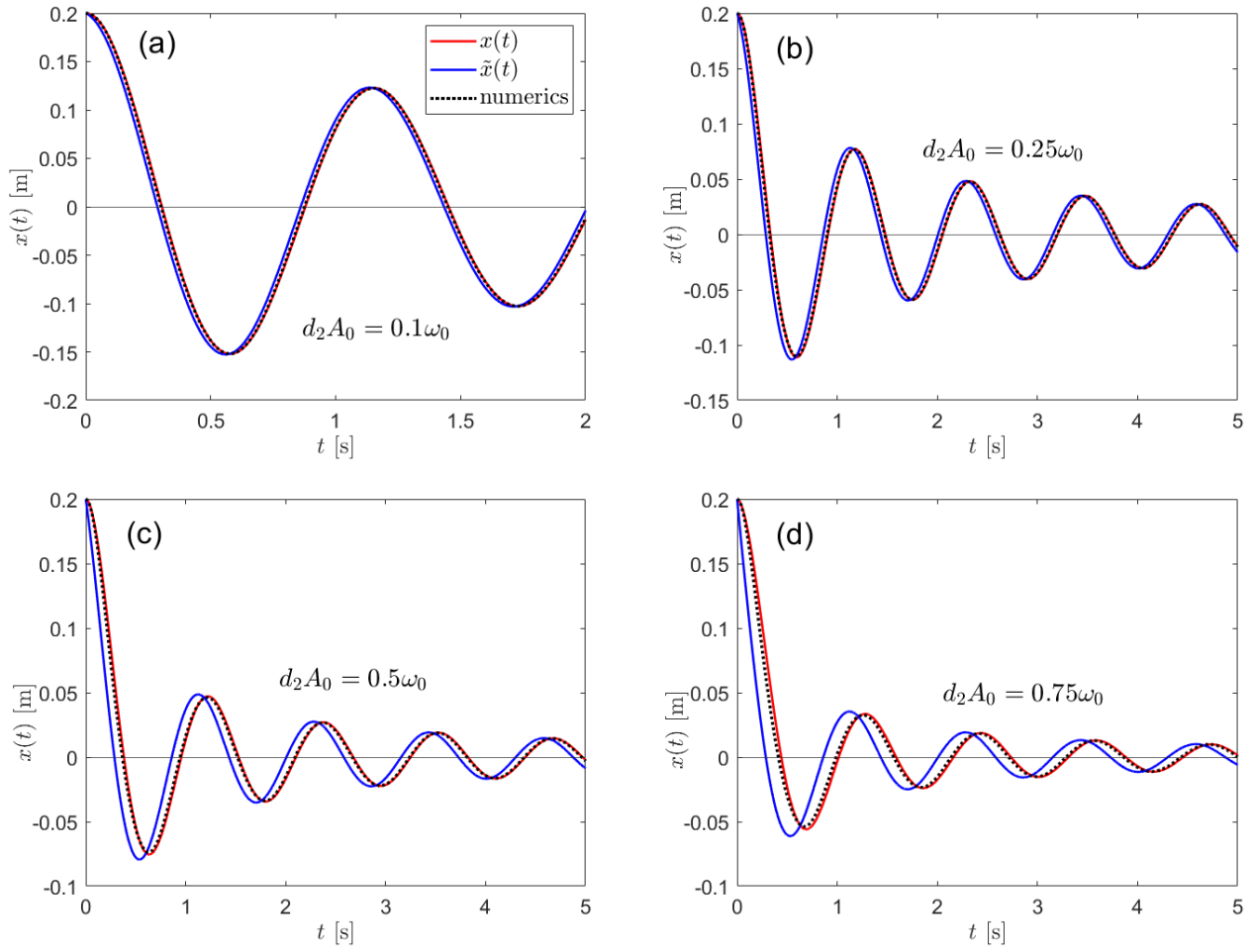


FIG. 2: Solid red curves show the solutions  $x(t)$  with initial conditions  $(x_0 = 0.2m, v_0 = 0)$  and various values of the ratio  $d_2A_0/\omega_0$ . Solid blue curves show the solutions  $\tilde{x}(t)$  and black dotted curves show the numerical solutions for the same initial conditions and the corresponding values of the ratio  $d_2A_0/\omega_0$ . See text for details.

We take here  $v_0 = \omega_0 A_0 = 1.10m/s$ . In Fig. 4(a) and (b) we show solutions (32) and the corresponding numerical solutions with initial conditions  $(x_0 = 0, v_0 = 1.10m/s)$  for  $d_2A_0/\omega_0 = \{0.25, 0.5\}$ . In Fig. 5(a) and (b) we show the corresponding energies given by (15) and (10), i.e.  $E(t)$  and  $\tilde{E}(t)$ , and numerically obtained energies. Therefore, as we commented earlier, although the new approach and the approach used in [14] give the same approximate analytical solutions in the case of initial conditions  $(x_0 = 0, v_0 \neq 0)$ , the corresponding energies differ even in this case, i.e. the energy is in general more realistically modeled in the new approach.

### C. Initial conditions $(x_0 \neq 0, v_0 \neq 0)$

As an example, here we take  $x_0 = A_0\sqrt{2}/2 = 0.14m$  and  $v_0 = -\omega_0 x_0 = -0.77m/s$ . For this choice, initial potential energy is equal to initial kinetic energy, and  $\varphi_0 = \pi/4$ . In Fig. 6(a) and (b) we show solutions  $x(t)$  given by (29), solutions  $\tilde{x}(t)$  given by (30), and the corresponding numerical solutions for  $d_2A_0/\omega_0 = \{0.25, 0.5\}$  with chosen initial conditions. In Fig. 7(a) and (b) we show the corresponding energies given by (15) and (10), i.e.  $E(t)$  and  $\tilde{E}(t)$ , and numerically obtained energies.

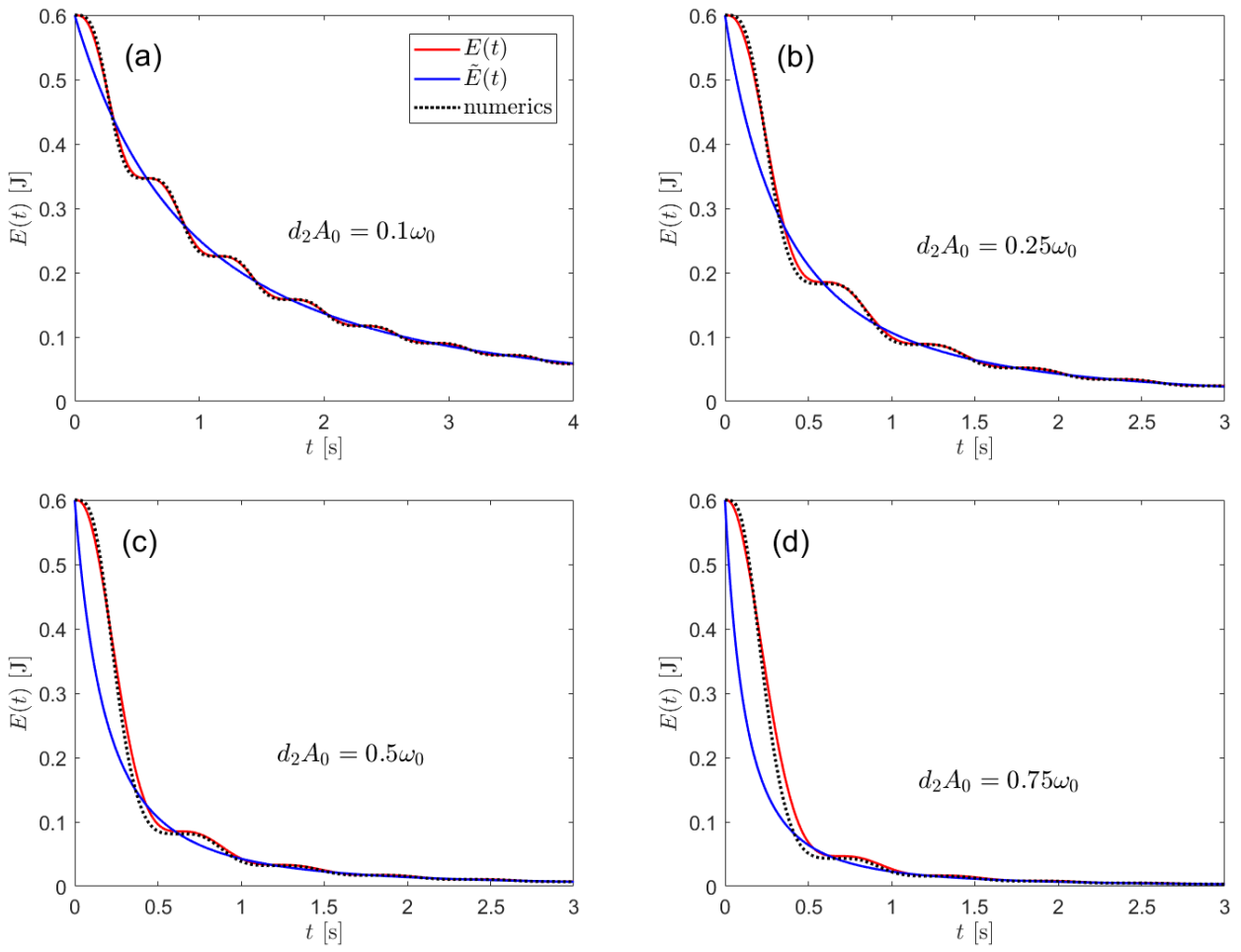


FIG. 3: Solid red curves show the energies  $E(t)$  with initial conditions ( $x_0 = 0.2m, v_0 = 0$ ) for the same values of the ratio  $d_2A_0/\omega_0$  as used in Fig. 2(a)-(d). Solid blue curves show the energies  $\tilde{E}(t)$  and black dotted curves show the numerically obtained energies with the same initial conditions and for the corresponding values of the ratio  $d_2A_0/\omega_0$ . See text for details.

#### D. Comments on results for harmonic oscillator with damping quadratic in velocity

The results presented in this section show that the new approximate analytical solutions, i.e. solutions (29) with initial amplitude (26) and initial phase (27), agree excellently with the numerical solutions in describing the free oscillations of a harmonic oscillator with damping quadratic in velocity for all types of initial conditions and for a range of values  $0 < D \lesssim 5.89 \text{ kg/m}$  of the corresponding damping constant, i.e. for  $0 < d_2A_0/\omega_0 \lesssim 0.5$ . For  $d_2A_0/\omega_0 > 0.5$  the deviations of the solutions (29) from the numerical solutions become more pronounced, as the example in Fig. 2(d), with  $D = 8.84 \text{ kg/m}$  (i.e.  $d_2A_0/\omega_0 = 0.75$ ), clearly shows.

Although the differential equation (20), which gives us the function  $f(t)$ , was derived under the assumption of weak damping, i.e. under the assumption  $|df(t)/dt| \ll \omega_0$ , we see that solutions (29) describe the dynamics well for damping that we could characterize (at least) as moderately strong. For example, in [21] the elliptic harmonic balance method has been used to obtain approximate analytical solutions of the harmonic oscillator with strong quadratic damping, and the parameters used were such that the amplitude of the obtained approximate analytical solution, as well as the corresponding numerical solution, after the first period drops to somewhat less than 50% of the initial value (see Fig. 6 in [21]). We can see, in Fig. 2(b), that for our choice of parameters, this happens for  $d_2A_0/\omega_0 = 0.25$ , and for  $d_2A_0/\omega_0 = 0.5$  the amplitude after the first period drops to slightly less than 25% of the initial value, as shown in Fig. 2(c). Therefore, although our derivation of the function  $f(t)$  is based on the assumption that it changes slowly with time relative to the oscillatory (trigonometric) part of the dynamics, which is strictly fulfilled only in the limit of weak damping, the solution we obtained describes the dynamics well even for rather strong damping.

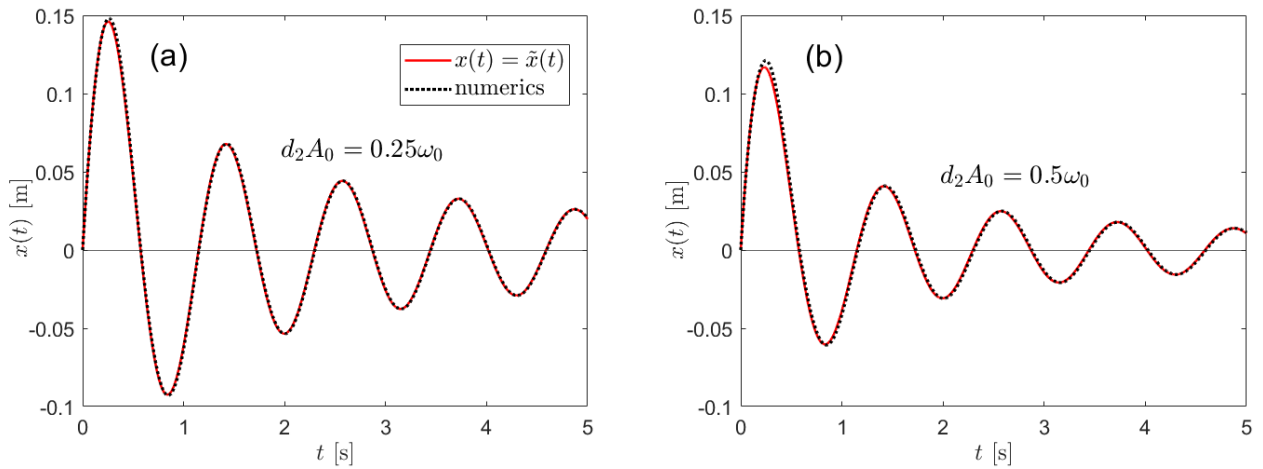


FIG. 4: Solid red curves show the solutions  $x(t)$  with initial conditions ( $x_0 = 0, v_0 = 1.10 \text{m/s}$ ) for two values of the ratio  $d_2 A_0 / \omega_0$ . Dotted black curves show the numerical solutions for the same initial conditions and the corresponding values of the ratio  $d_2 A_0 / \omega_0$ . See text for details.

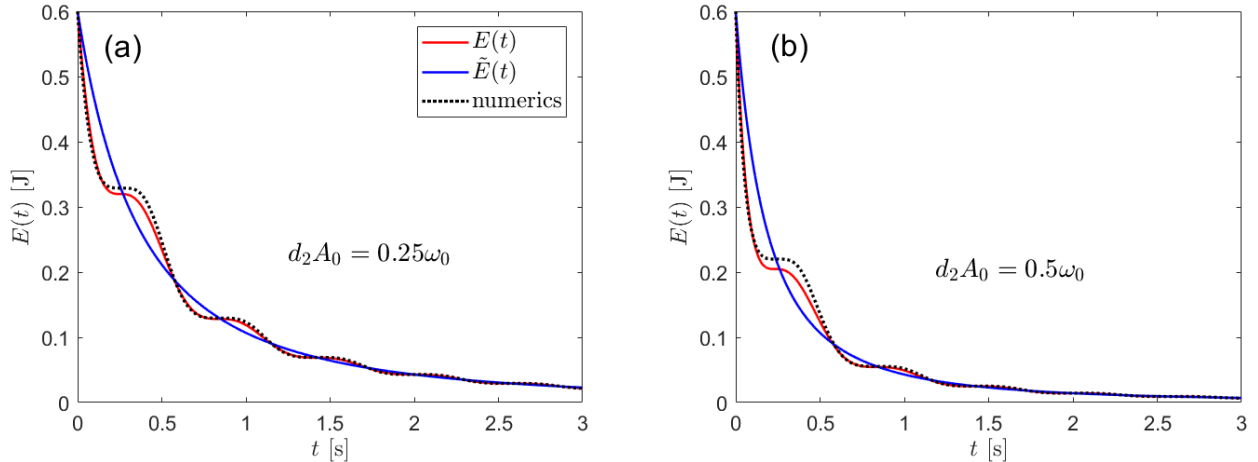


FIG. 5: Solid red curves show the energies  $E(t)$  with initial conditions ( $x_0 = 0, v_0 = 1.1 \text{m/s}$ ) for the same values of the ratio  $d_2 A_0 / \omega_0$  as used in Fig. 4(a) and (b). Solid blue curves show the energies  $\tilde{E}(t)$  and black dotted curves show the numerically obtained energies with the same initial conditions and for the corresponding values of the ratio  $d_2 A_0 / \omega_0$ . See text for details.

Furthermore, an ansatz of similar form as (11) is used in [22], but with an unknown frequency (i.e. with  $\omega \neq \omega_0$ ) and, by a more complex mathematical procedure, which also includes the time averaging over the trigonometric part of the ansatz, approximate solutions of the harmonic oscillator with damping quadratic in velocity were obtained with a frequency that is reduced in relation to the frequency of the undamped case. More precisely, the obtained frequency is  $\omega = \omega_0 - \Delta\omega_0$  [22], where  $\Delta\omega_0 > 0$  is the term which depends on the constant of quadratic damping  $D$  and on magnitude of the initial amplitude. A brief numerical analysis of the free oscillations of the harmonic oscillator with damping quadratic in velocity presented in [14] shows, for initial condition ( $x_0 > 0, v_0 = 0$ ) and  $0 < d_2 A_0 / \omega_0 \leq 0.5$ , that the quadratic damping has the greatest effect on the shift of the instants of the first zero crossing and the first turning point, while the time interval between the subsequent turning points remains approximately equal to the half-period of the undamped oscillator. Thus, the dynamics can be described well by keeping the frequency the same as in the undamped case, and taking into account that the initial phase can change compared to the undamped case, as we have done here.

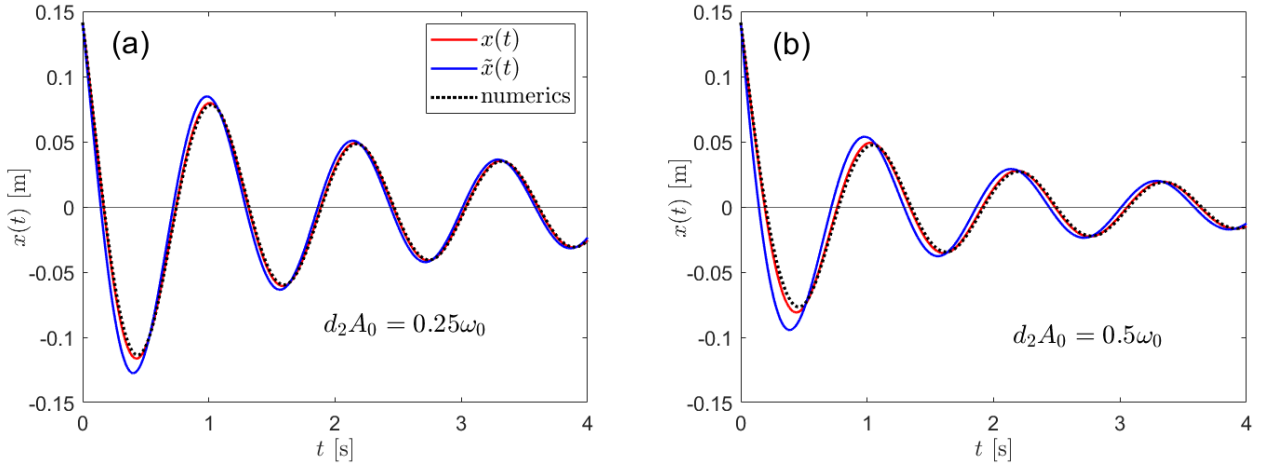


FIG. 6: Solid red curves show the solutions  $x(t)$  with initial conditions ( $x_0 = 0.14m$ ,  $v_0 = -0.77m/s$ ) for two values of the ratio  $d_2A_0/\omega_0$ . Solid blue curves show the solutions  $\tilde{x}(t)$  and black dotted curves show the numerical solutions for the same initial conditions and the corresponding values of the ratio  $d_2A_0/\omega_0$ . See text for details.

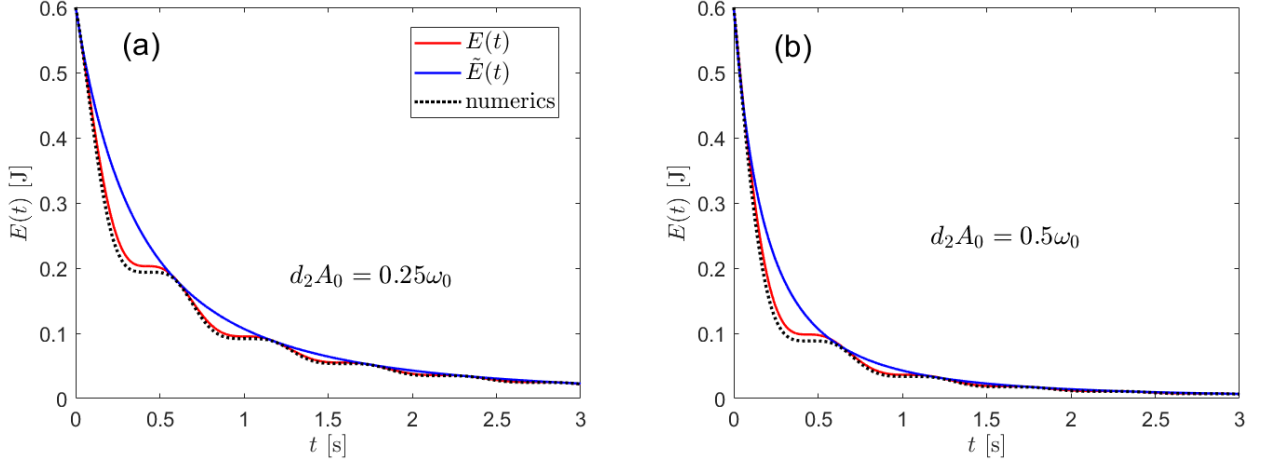


FIG. 7: Solid red curves show the energies  $E(t)$  with initial conditions ( $x_0 = 0.14$ ,  $v_0 = -0.77m/s$ ) for the same values of the ratio  $d_2A_0/\omega_0$  as used in Fig. 6(a) and (b). Solid blue curves show the energies  $\tilde{E}(t)$  and black dotted curves show the numerically obtained energies with the same initial conditions and for the corresponding values of the ratio  $d_2A_0/\omega_0$ . See text for details.

#### IV. COULOMB DAMPING

If  $\mu > 0$  and  $D = b = 0$  (i.e.  $d_0 > 0$  and  $d_1 = d_2 = 0$ ), equation (22) becomes a (depressed) quartic equation in  $A$ , i.e.

$$\omega_0^2 A^4 - (v_0^2 + \omega_0^2 x_0^2) A^2 - 2x_0 v_0 d_0 A - d_0^2 x_0^2 = 0, \quad (33)$$

while equation (23) simplifies to

$$\varphi = \arctan \left( -\frac{v_0 + x_0 d_0 / A}{\omega_0 x_0} \right). \quad (34)$$

In this case solving integral (24) gives

$$f(t) = 1 - \frac{d_0}{A} t. \quad (35)$$

The function (35) monotonically decreases from the value  $f(0) = 1$  to  $f(\tau) = 0$ , where  $\tau = A/d_0$ . For  $t > \tau$ , (35) becomes increasingly negative, which corresponds to an increase in the amplitude of oscillations and is not physical. Thus, in the case of Coulomb damping, our approximate solution (11) can be written as

$$x(t) = (A - d_0 t) \theta(t) \cos(\omega_0 t + \varphi), \quad (36)$$

where

$$\theta(t) = \begin{cases} 1 & \text{if } 0 \leq t \leq \tau \\ 0 & \text{if } t > \tau, \end{cases} \quad (37)$$

while  $A$  is obtained by solving (33) and  $\varphi$  calculated from (34). The corresponding velocity, i.e. (12), can be written as

$$v(t) = (-\omega_0 (A - d_0 t) \sin(\omega_0 t + \varphi) - d_0 \cos(\omega_0 t + \varphi)) \theta(t), \quad (38)$$

Thus, the function  $\theta(t)$  is simply added by hand to exclude the non-physical part of the solution. In this case, the approach used in [14] gives

$$\tilde{x}(t) = (A_0 - d_0 t) \tilde{\theta}(t) \cos(\omega_0 t + \varphi_0), \quad (39)$$

where  $\tilde{\theta}(t)$  is the same as (37) but with  $\tilde{\tau} = A_0/d_0$  instead of  $\tau$ . It is well known that the exact solutions of a harmonic oscillator with Coulomb damping halt at some finite time instant  $t_{halt}$  and, in general, at some displacement  $x_{halt} \neq 0$  with property  $|x_{halt}| \leq \mu mg/k$ , e.g., see [5–7, 14, 23]. The approximate solution (36) describes the dynamics up to the instant  $t = \tau$ , at which  $x(\tau) = 0$  and the corresponding velocity, given by (38), is  $v(\tau) \neq 0$ . Thus, if we take  $\tau$  as an approximation of  $t_{halt}$ , in addition to an error in the halting position, our modeled solution (36) has an error in velocity. In case of solution (39), there is also an error in the halting position, since  $\tilde{x}(\tilde{\tau}) = 0$ , but the corresponding velocity, given by (9), is  $\tilde{v}(\tilde{\tau}) = 0$ , i.e. it has the correct value at least from a modeling point of view. We will first show examples with solutions (36) and (39) as they are, and then introduce an alternative approach that corrects the aforementioned shortcomings of solution (36).

Since the exact solutions of the harmonic oscillator with Coulomb damping are piecewise continuous and have already been studied in detail elsewhere, e.g., see [5–7, 14, 23], for simplicity, we will again check the validity of our approximate solutions by comparing them with numerically obtained solutions.

### A. Initial conditions ( $x_0 > 0, v_0 = 0$ )

For this type of initial conditions, equation (33) reduces to a quadratic equation in  $A^2$  and we easily get

$$A = \sqrt{\frac{x_0^2 + \sqrt{x_0^4 + 4(d_0 x_0 / \omega_0)^2}}{2}} \quad \text{and} \quad \varphi = \arctan\left(-\frac{d_0}{\omega_0 A}\right). \quad (40)$$

In Fig. 8(a) and (b) we show solutions  $x(t)$  given by (36), solutions  $\tilde{x}(t)$  given by (39) and the corresponding numerical solutions with initial conditions ( $x_0 = 0.2m, v_0 = 0$ ) for  $\mu = \{0.048, 0.096\}$ , i.e. for  $d_0/(\omega_0 A_0) = \{0.05, 0.1\}$ . In case  $d_0/(\omega_0 A_0) = 0.05$ , relations (40) give  $A = 0.2002m \approx A_0$  and  $\varphi = -0.05 \approx \varphi_0$ . Thus, solutions (36) and (39) almost completely overlap in Fig. 8(a). Even for a rather strong Coulomb damping with  $d_0/(\omega_0 A_0) = 0.1$ , shown in Fig. 8(b), the amplitude  $A = 0.201m \approx A_0$ , but the phase becomes more clearly visible, i.e.  $\varphi = -0.1$ , and we see that the solution  $x(t)$  agrees somewhat better with the numerical solution than the solution  $\tilde{x}(t)$  when considering the overall dynamics, but the improvement is not significant.

The dashed horizontal lines in Fig. 8(a) and (b) indicate the region within which  $k|x(t)| \leq \mu mg$  holds, i.e. the region in which the restoring force is of smaller magnitude than the friction force. In both Fig. 8(a) and (b) we see that the approximate solutions have the last turning point within the area marked by the two dashed lines. After the last turning point, our approximate solutions describe the motion that continues until the block reaches the equilibrium position. In addition to the error in the halting positions, in Fig. 8(a) and (b) we see that solutions  $x(t)$  and  $\tilde{x}(t)$  also have errors in the instants of the zero crossings compared to the numerical solutions, and we can see that these errors increase with time, therefore the largest error is for the last zero crossing (the fact that solutions of the form (39) have errors in instants of zero crossings compared to exact analytical solutions of the harmonic oscillator with Coulomb damping is argued in [14], and the same argument can be applied to solutions of the form (36)). One way to make our description of the dynamics more physical would be simply to take that the dynamics halts when the

approximate solutions reach the last turning point. In the examples shown in Fig. 8(a) and (b), we see that this would somewhat reduce the error in the halting position, but would not affect the rather large error in the instant of the last zero crossing. Thus, to improve the agreement between the solutions of the form (36) and the numerical solutions, we will apply a slightly different strategy.

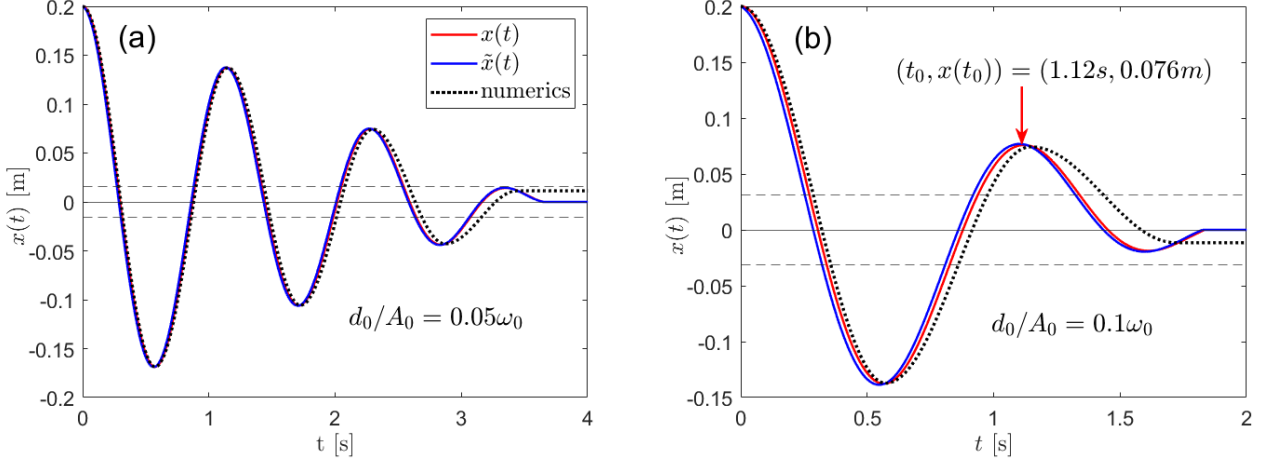


FIG. 8: Solid red curves show the solutions  $x(t)$  with initial conditions ( $x_0 = 0.2m, v_0 = 0$ ) for two values of the ratio  $d_0/(A_0\omega_0)$ . Solid blue curves show the solutions  $\tilde{x}(t)$  and black dotted curves show the numerical solutions for the same initial conditions and the corresponding values of the ratio  $d_0/(A_0\omega_0)$ . The dashed horizontal lines in each figure are positioned at corresponding  $\pm\mu mg/k$  values, i.e. they indicate the region within which  $|x(t)| \leq \mu mg/k$  holds. See text for details.

In Fig. 8(b), as an example, the red arrow points to  $(t_0, x(t_0)) = (1.12s, 0.076m)$ , i.e. to the last turning point of the solution  $x(t)$  for which  $k|x(t_0)| > \mu mg$  holds. We can take that solution (36) describes the dynamics for  $0 \leq t \leq t_0$ , and to describe the dynamics for  $t > t_0$ , we exactly solve the equation of motion with the initial conditions  $(x(t_0) \neq 0, v(t_0) = 0)$ . We get

$$x(t) = \begin{cases} (A - d_0 t) \cos(\omega_0 t + \varphi) & \text{if } 0 \leq t \leq t_0 \\ (x(t_0) - \text{sgn}[x(t_0)] \frac{\mu mg}{k}) \cos(\omega_0(t - t_0)) + \text{sgn}[x(t_0)] \frac{\mu mg}{k} & \text{if } t_0 < t \leq t_0 + \pi/\omega_0 \\ -x(t_0) + 2 \text{sgn}[x(t_0)] \frac{\mu mg}{k} & \text{if } t > t_0 + \pi/\omega_0 \end{cases} \quad (41)$$

as the improved approximate solution, and

$$v(t) = \begin{cases} -\omega_0(A - d_0 t) \sin(\omega_0 t + \varphi) - d_0 \cos(\omega_0 t + \varphi) & \text{if } 0 \leq t \leq t_0 \\ -\omega_0(x(t_0) - \text{sgn}[x(t_0)] \frac{\mu mg}{k}) \sin(\omega_0(t - t_0)) & \text{if } t_0 < t \leq t_0 + \pi/\omega_0 \\ 0 & \text{if } t > t_0 + \pi/\omega_0 \end{cases} \quad (42)$$

as the corresponding velocity. Therefore, our strategy is as follows: knowing the function  $(A - d_0 t) \cos(\omega_0 t + \varphi)$ , we can easily read out, for any choice of initial conditions and any value of the ratio  $d_0/(\omega_0 A_0)$ , the values of  $t_0$  and  $x(t_0)$ , i.e. the values corresponding to the last turning point with the property  $k|x(t_0)| > \mu mg$ , and use these values in relations (41) and (42). In Fig. 9(a) and (b) we show improved solutions  $x(t)$  given by (41), solutions  $\tilde{x}(t)$  given by (39) and the corresponding numerical solutions for the same initial conditions and ratios  $d_0/(\omega_0 A_0)$  as used in Fig. 8(a) and (b). We see that solution (41) is in excellent agreement with the numerical solution, i.e. it gives an excellent approximation of the halting position, and the time  $t_0 + \pi/\omega_0$  is an excellent approximation of the duration of motion. In Fig. 10(a) and (b) we show the energy  $E(t) = kx(t)^2/2 + mv(t)^2/2$  obtained using (41) and (42), energy  $\tilde{E}(t) = m\omega_0^2(A_0 - d_0 t)^2\tilde{\theta}(t)/2$  corresponding to solution (39), and the numerically obtained energy for the same initial conditions and ratios  $d_0/(\omega_0 A_0)$  as used in Fig. 9(a) and (b). We can see that energy  $E(t)$ , in addition to modeling the energy behavior more realistically compared to energy  $\tilde{E}(t)$ , is in excellent agreement with the numerically obtained energy.

Our approximate analytical solution (41) is piecewise continuous, but it is necessary to consider only two time intervals, i.e.  $0 \leq t \leq t_0$  and  $t_0 < t \leq t_0 + \pi/\omega_0$ , while the exact solution of the harmonic oscillator with Coulomb damping describes the dynamics over half periods [5–7, 14, 23]. For example, in Fig. 11(a) we show the solutions

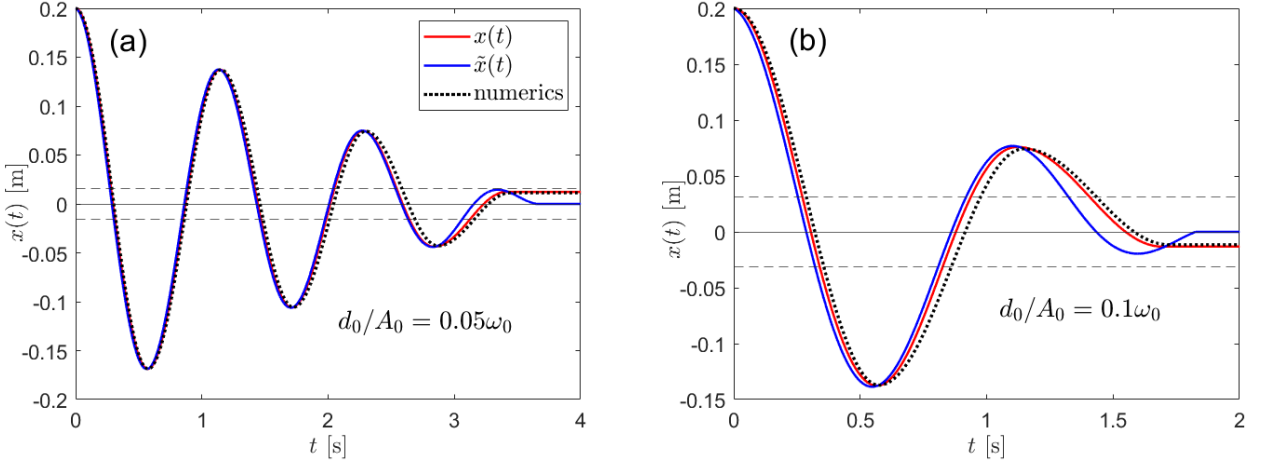


FIG. 9: Solid red curves show the solutions (41) with initial conditions ( $x_0 = 0.2\text{m}$ ,  $v_0 = 0$ ) for two values of the ratio  $d_0/(A_0\omega_0)$ . Solid blue curves show the solutions  $\tilde{x}(t)$ , given by (39), and black dotted curves show the numerical solutions for the same initial conditions and the corresponding values of the ratio  $d_0/(A_0\omega_0)$ . The dashed horizontal lines in each figure are positioned at corresponding  $\pm\mu mg/k$  values, i.e. they indicate the region within which  $|x(t)| \leq \mu mg/k$  holds. See text for details.

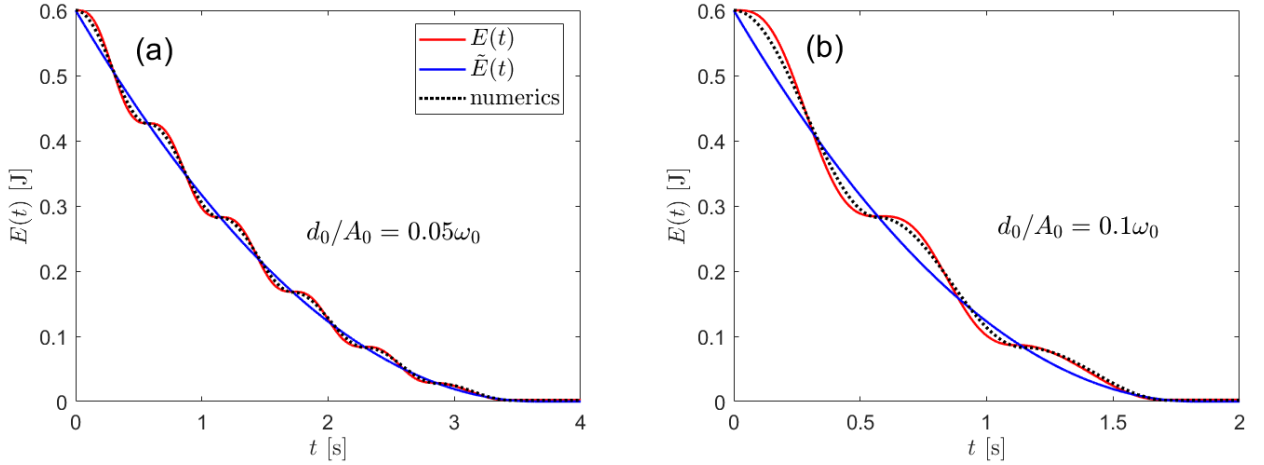


FIG. 10: Solid red curves show the energies  $E(t)$ , obtained using (41) and (42), for the same initial conditions and values of the ratio  $d_0/A_0\omega_0$  as used in Fig. 9(a) and (b). Solid blue curves show the energies  $\tilde{E}(t) = m\omega_0^2(A_0 - d_0t)^2\tilde{\theta}(t)/2$  corresponding to solutions (39), and black dotted curves show the numerically obtained energies, both for the same initial conditions and values of the ratio  $d_0/A_0\omega_0$  as used for  $E(t)$ . See text for details.

(41), (39) and the corresponding numerical solutions for  $d_0/(\omega_0 A_0) = 0.03$  (i.e. for  $\mu = 0.029$ ). In this case, an exact analytical solution would require considering the dynamics over eleven time intervals, i.e. eleven half-periods, while, as we said, solution (41) considers only two time intervals and agrees excellently with the numerically obtained solution. In Fig. 11(b) we show the energies corresponding to solutions shown in Fig. 11(a).

## B. Initial conditions ( $x_0 = 0, v_0 > 0$ )

For this type of initial conditions, equation (33) simplifies to  $A = A_0 = v_0/\omega_0$  and we get  $\varphi = \varphi_0 = -\pi/2$ , i.e. (36) and (39) become equal. The improved solution, i.e. (41), is, of course, also valid for these initial conditions, it is only necessary to determine the values  $(t_0, x(t_0))$  of the last turning point of the function  $(A_0 - d_0t) \cos(\omega_0 t + \varphi)$  with property  $|x(t_0)| > \mu mg/k$ , and insert these values into expression (41). For example, in Fig. 12(a) we show the solutions

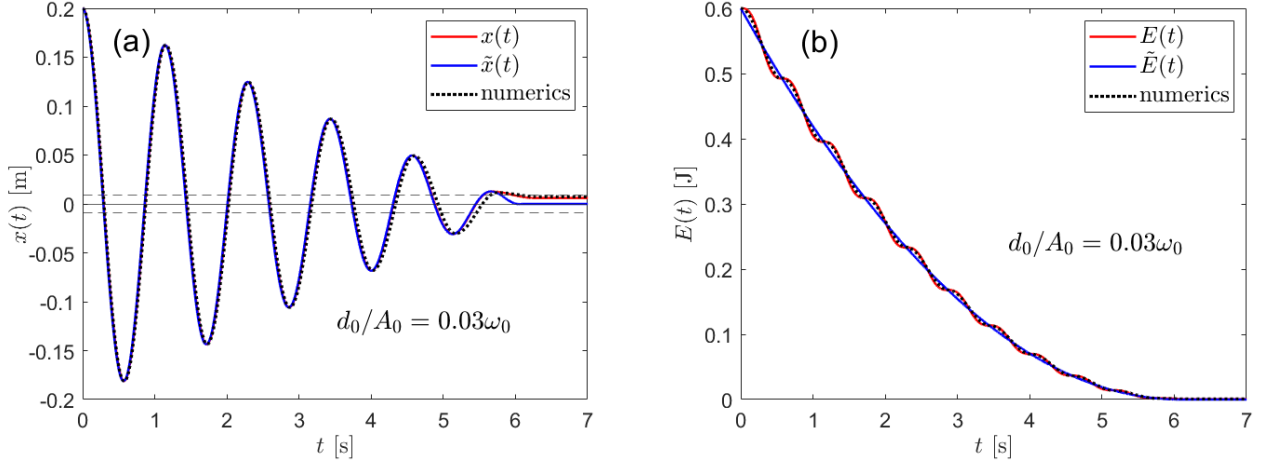


FIG. 11: (a) Solid red curves show the solution (41) with initial conditions ( $x_0 = 0.2m, v_0 = 0$ ) and  $d_0/(A_0\omega_0) = 0.03$ . Solid blue curves show the corresponding solution (39) and black dotted curves show the corresponding numerical solution. The dashed horizontal lines are positioned at  $\pm \mu mg/k$ , i.e. they indicate the region within which  $|x(t)| \leq \mu mg/k$  holds. (b) The energies corresponding to solutions shown in figure (a). See text for details.

(41), (39) and the corresponding numerical solutions for this choice of the initial conditions and  $d_0/(\omega_0 A_0) = 0.05$ . In this case, solutions (41) and (39) overlap for  $0 < t \leq t_0$ , and for  $t > t_0$  the solution (41) agrees significantly better with the numerical solution. In Fig. 12(b) we show the energies corresponding to solutions shown in Fig. 12(a).

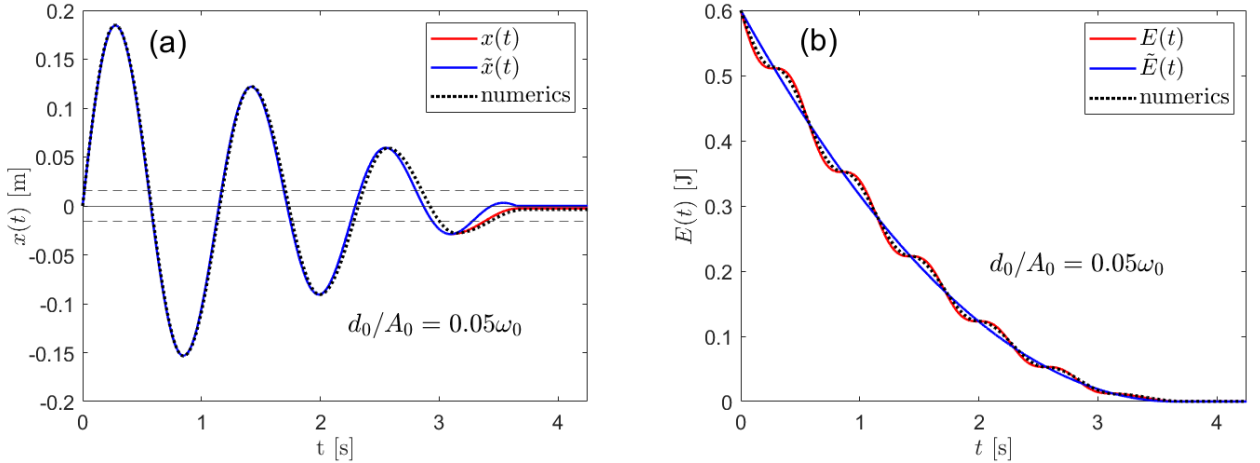


FIG. 12: (a) Solid red curves show the solution (41) with initial conditions ( $x_0 = 0, v_0 = \omega_0 A_0$ ) and  $d_0/(\omega_0 A_0) = 0.05$ . Solid blue curves show the corresponding solution (39) and black dotted curves show the corresponding numerical solution. The dashed horizontal lines are positioned at  $\pm \mu mg/k$ , i.e. they indicate the region within which  $|x(t)| \leq \mu mg/k$  holds. (b) The energies corresponding to solutions shown in figure (a). See text for details.

### C. Initial conditions ( $x_0 \neq 0, v_0 \neq 0$ )

As an example, here we choose ( $x_0 = A_0\sqrt{2}/2, v_0 = \omega_0 x_0$ ) and  $d_0/(\omega_0 A_0) = 0.05$ . For this type of initial conditions, equation (33) remains a quartic equation in  $A$ , i.e. we have to solve

$$30A^4 - 1.200A^2 - 0.012A - 6 \times 10^{-5} = 0,$$

where we did not write the physical units for simplicity and the resulting  $A$  is in meters. Instead of delving into solving this quartic equation analytically, we solve it using the *roots* MATLAB function. We get four solutions, i.e.  $A/m = \{0.205, -0.195, -0.005 + i0.005, -0.005 - i0.005\}$ . We expected one of the solutions to be close to  $A_0 = 0.2m$ , therefore we take the value  $A = 0.205m$  as our solution, and the corresponding phase (34) is  $\varphi = -0.809$ . In Fig. 13(a) we show the solutions (41), (39) and the numerical solutions corresponding to this choice of the initial conditions and value of the ratio  $d_0/(\omega_0 A_0)$ . In Fig. 13(b) we show the energies corresponding to solutions shown in Fig. 13(a).

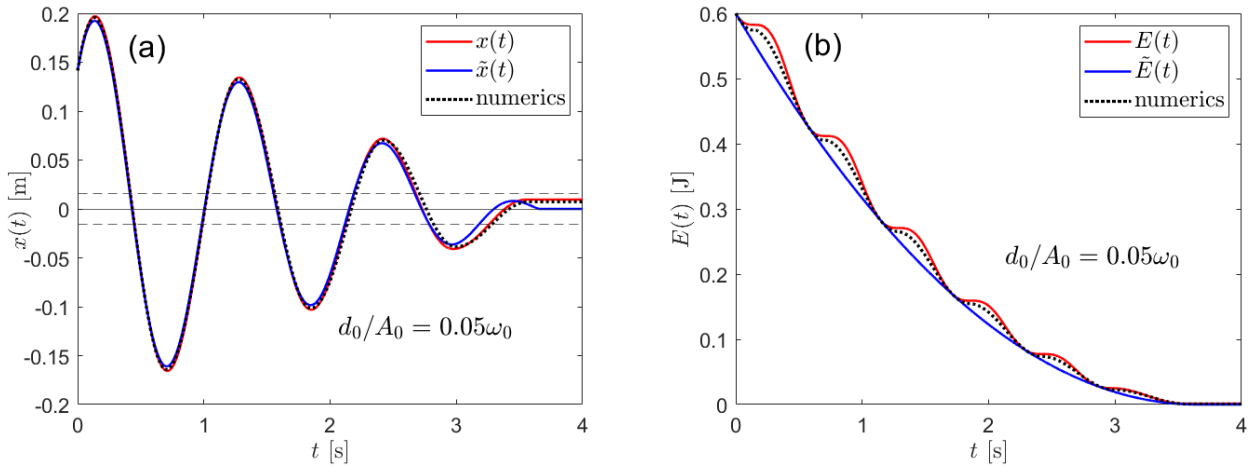


FIG. 13: (a) Solid red curves show the solution (41) with initial conditions ( $x_0 = A_0\sqrt{2}/2, v_0 = \omega_0 x_0$ ) and  $d_0/(A_0\omega_0) = 0.05$ . Solid blue curves show the corresponding solution (39) and black dotted curves show the corresponding numerical solution. The dashed horizontal lines are positioned at  $\pm\mu mg/k$ , i.e. they indicate the region within which  $|x(t)| \leq \mu mg/k$  holds. (b) The energies corresponding to solutions shown in figure (a). See text for details.

#### D. Comments on results for harmonic oscillator with Coulomb damping

The results presented in this section show that, in the case of Coulomb damping, the new approximate analytical solutions, i.e. solutions (36) with the corresponding  $A$  and  $\varphi$ , do not provide a significantly better description of the dynamics compared to the solutions (39) which are provided by the approach used in [14]. In order to obtain a better agreement between the approximate analytical solutions (36) and the numerical solutions, we improved them by using (36) to describe the dynamics only up to the instant  $t_0$ , which corresponds to the last turning point with displacement  $|x(t_0)| > \mu mg/k$ , while the description of the dynamics for  $t > t_0$  is obtained by solving exactly the equation of motion with the initial conditions ( $x(t_0) \neq 0, v(t_0) = 0$ ), i.e. we introduced improved approximate analytical solution (41). We showed that solution (41) gives excellent description of free oscillations of the harmonic oscillator with Coulomb damping for any type of initial conditions and for a range of corresponding damping constant  $0 < \mu \leq 0.048$ , i.e. for  $0 < d_0/(\omega_0 A_0) \leq 0.05$ .

As we have already mentioned, the case of free oscillations of the harmonic oscillator with Coulomb damping is exactly solvable, but the exact solution is piecewise continuous, i.e. it is necessary to analyze the dynamics over half-periods. Thus, the main advantage of the approximate analytical solution (41), compared to the exact solution, is that it requires us to consider only two time intervals, i.e.  $0 \leq t \leq t_0$  and  $t_0 < t \leq t_0 + \pi/\omega_0$ . This advantage is lost as we consider increasingly stronger Coulomb damping. For example, in Fig. 9(b), we see that even for a rather strong damping with  $d_0/(\omega_0 A_0) = 0.1$ , for which the amplitude after the first period drops to a value less than 50% of the initial value, the approximate analytical solution (41) follows the numerical solution well, but in this example the advantage of solution (41) compared to the exact solution would not be great, i.e. solution (41) is written over two time intervals, while the corresponding exact solution would be written over three time intervals (three half-periods).

We note here that approximate analytical solutions (36) and (39), for the range of values  $0 < d_0/(\omega_0 A_0) \leq 0.05$ , both begin to deviate significantly from the numerical solutions only after their corresponding energies, as well as the numerically obtained energies, drop to a small fraction of the initial energy, e.g. for  $d_0/(\omega_0 A_0) = 0.05$  to about 5% of initial energy, i.e. towards the very end of the dynamics. Thus, if we do not need high precision in describing the very end of the dynamics, both solutions (36) and (39) provide an elegant description of the overall dynamics and a solid estimate of the duration of the motion.

## V. COMBINED QUADRATIC AND COULOMB DAMPING

If  $\mu > 0$ ,  $D > 0$  and  $b = 0$  (i.e.  $d_0 > 0$ ,  $d_2 > 0$  and  $d_1 = 0$ ), equation (22) becomes a quartic equation in  $A$ , i.e.

$$(\omega_0^2 - x_0^2 d_2^2) A^4 - 2x_0 v_0 d_2 A^3 - (v_0^2 + \omega_0^2 x_0^2 + 2d_0 d_2 x_0^2) A^2 - 2x_0 v_0 d_0 A - d_0^2 x_0^2 = 0, \quad (43)$$

while the initial phase (23) becomes

$$\varphi = \arctan \left( -\frac{v_0 + (d_2 A + d_0/A)x_0}{\omega_0 x_0} \right). \quad (44)$$

In this case, solving the integral (24) gives

$$f(t) = \sqrt{\frac{d_0}{d_2 A^2}} \tan \left( -\sqrt{d_0 d_2} t + \arctan \left( \sqrt{\frac{d_2 A^2}{d_0}} \right) \right). \quad (45)$$

Similarly as in the case of purely Coulomb damping, the function (35) monotonically decreases from the value  $f(0) = 1$  to  $f(\tau) = 0$ , where

$$\tau = \frac{1}{\sqrt{d_0 d_2}} \arctan \left( \sqrt{\frac{d_2 A^2}{d_0}} \right). \quad (46)$$

For  $t > \tau$ , (45) becomes increasingly negative. Thus, our approximate solution (11) becomes

$$x(t) = \sqrt{\frac{d_0}{d_2}} \tan \left( -\sqrt{d_0 d_2} t + \arctan \left( \sqrt{\frac{d_2 A^2}{d_0}} \right) \right) \theta(t) \cos(\omega_0 t + \varphi), \quad (47)$$

where  $\theta(t)$  is defined as in (37), but with  $\tau$  given by (46), while  $A$  is obtained by solving (43) and  $\varphi$  calculated from (44). The velocity corresponding to (47) is

$$v(t) = \left( -\omega_0 A f(t) \sin(\omega_0 t + \varphi) + A \frac{df(t)}{dt} \cos(\omega_0 t + \varphi) \right) \theta(t), \quad (48)$$

where  $f(t)$  is given by (45), and the corresponding energy  $E(t) = kx(t)^2/2 + mv(t)^2/2$  is calculated with (47) and (48). In this case, the approach used in [14] gives  $\tilde{f}(t)$  of the same form as (45), but with  $A_0$  in place of  $A$ , i.e. approximate solution (8) becomes

$$\tilde{x}(t) = \sqrt{\frac{d_0}{d_2}} \tan \left( -\sqrt{d_0 d_2} t + \arctan \left( \sqrt{\frac{d_2 A_0^2}{d_0}} \right) \right) \tilde{\theta}(t) \cos(\omega_0 t + \varphi_0), \quad (49)$$

where  $\tilde{\theta}(t)$  is the same as  $\theta(t)$  but with  $\tilde{\tau} = \arctan(\sqrt{d_2 A_0^2/d_0})/\sqrt{d_0 d_2}$  instead of  $\tau$ . In the approach used in [14], the velocity corresponding to (49) is

$$\tilde{v}(t) = -\omega_0 A_0 \tilde{f}(t) \sin(\omega_0 t + \varphi_0) \tilde{\theta}(t), \quad (50)$$

and the corresponding energy is  $\tilde{E}(t) = k\tilde{x}(t)^2/2 + m\tilde{v}(t)^2/2 = m\omega_0^2 A_0^2 \tilde{f}(t)^2 \tilde{\theta}(t)/2$ .

### A. Initial conditions ( $x_0 > 0, v_0 = 0$ )

For this type of initial conditions, equation (43) reduces to a quadratic equation in  $A^2$  and we easily get

$$A = \sqrt{\frac{(\omega_0^2 + 2d_0 d_2)x_0^2 + \sqrt{(\omega_0^2 + 2d_0 d_2)^2 x_0^4 + 4d_0^2 d_2^2 (\omega_0^2 - d_2^2 x_0^2)}}{2(\omega_0^2 - d_2^2 x_0^2)}} \quad \text{and} \quad \varphi = \arctan \left( -\frac{d_2 A + d_0/A}{\omega_0} \right). \quad (51)$$

In Fig. 14(a)-(d) we show solutions  $x(t)$  given by (47), solutions  $\tilde{x}(t)$  given by (49) and the corresponding numerical solutions for  $d_0/(\omega_0 A_0) = \{0.01, 0.03\}$  and  $d_2 A_0/\omega_0 = \{0.15, 0.25\}$ , with initial conditions ( $x_0 = 0.2m, v_0 = 0$ ). In case  $d_0/(\omega_0 A_0) = 0.01$ , the error of our approximate solutions (47) and (49) in the halting position compared to the numerical solutions can be at most  $\Delta x = \pm \mu mg/k = \pm 0.016 x_0$ , while in case  $d_0/(\omega_0 A_0) = 0.03$  it can be at most  $\Delta x = \pm 0.047 x_0$ . In Fig. 14(a) and (b), we can see that for most of the time, solutions  $x(t)$  overlap perfectly with the numerical solutions, that is, only towards the end of the motion are the deviations from the numerical solutions noticeable, mostly at the instants of the last zero crossings and, of course, at the instants and the positions of the halt. These discrepancies occur due to the presence of Coulomb damping, and in Fig. 14(c) and (d) are more pronounced, due to stronger Coulomb damping. In Fig. 15(a)-(d) we show the energies corresponding to solutions shown in Fig. 14(a)-(d). We see that the energies corresponding to the solution (47) are in excellent agreement with the numerically obtained energies. Thus, the deviations of the solutions (47) from the numerical solutions towards the end of the dynamics, which we can see in Fig. 14(a)-(d), are negligible in the context of energy.

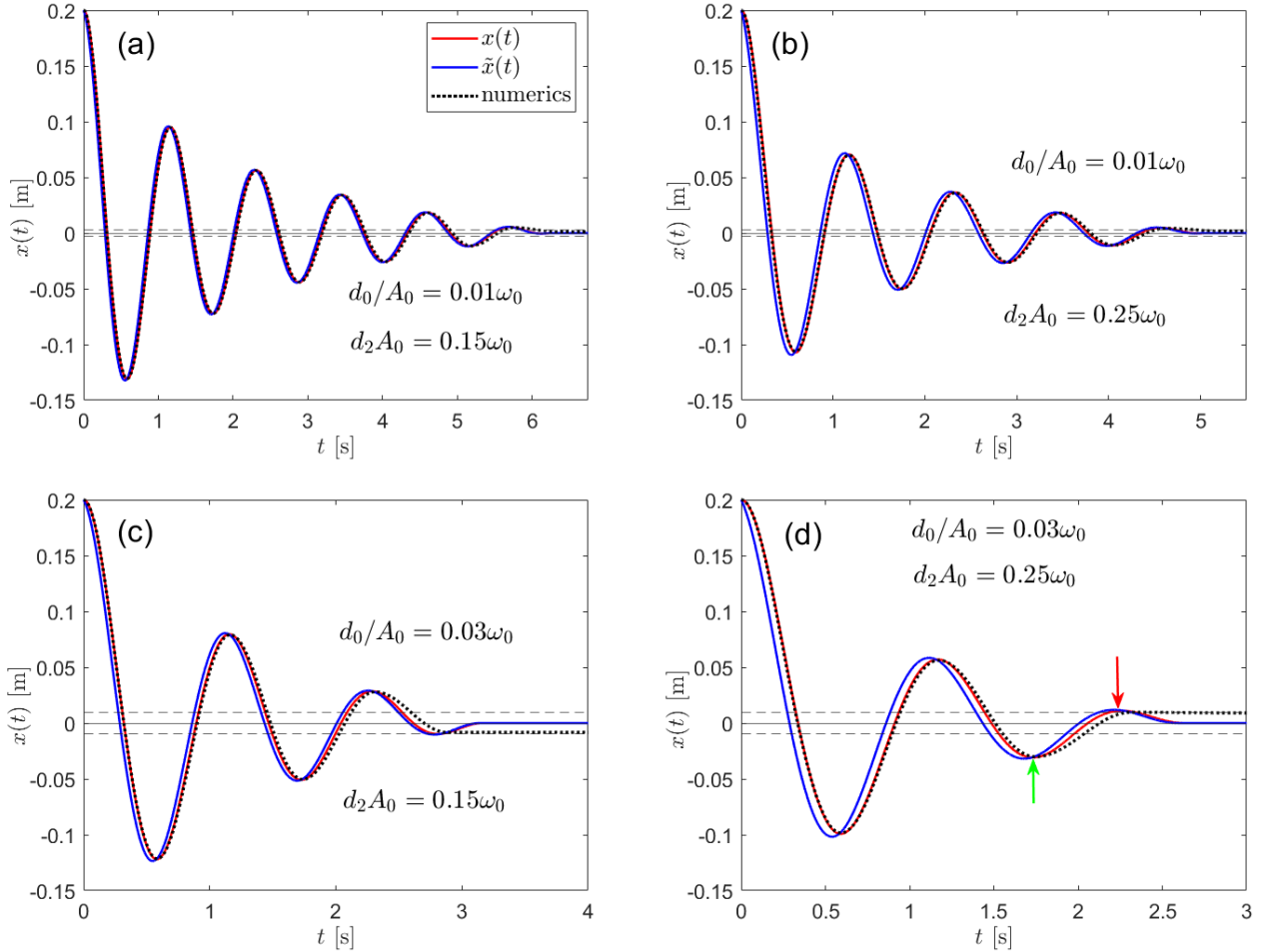


FIG. 14: Solid red curves show the solutions  $x(t)$ , given by (47), with initial conditions ( $x_0 = 0.2m, v_0 = 0$ ) for  $d_0/(\omega_0 A_0) = \{0.01, 0.03\}$  and  $d_2 A_0/\omega_0 = \{0.15, 0.25\}$ . Solid blue curves show the solutions  $\tilde{x}(t)$ , given by (49), and black dotted curves show the numerical solutions for the same initial conditions and the corresponding values of the ratios  $d_0/(\omega_0 A_0)$  and  $d_2 A_0/\omega_0$ . The dashed horizontal lines in each figure are positioned at corresponding  $\pm \mu mg/k$  values, i.e. they indicate the region within which  $|x(t)| \leq \mu mg/k$  holds. See text for details.

Still, in order to make our approximate description of dynamics, i.e. the solution (47), a better model of physical reality, we will proceed similarly as in the case with purely Coulomb damping. As an example, the red arrow in Fig. 14(d) points to  $(t_0, x(t_0)) = (2.37s, 0.049x_0)$ , i.e. to the last turning point of the solution (47) with the magnitude of displacement greater than  $\mu mg/k = 0.047x_0$ . In this particular case, the displacement of the considered turning point, i.e.  $x(t_0)$ , is only 4% larger in magnitude than  $\mu mg/k$ . For this reason, it is barely visible in Fig. 14(d) that this turning point is above the dashed horizontal line. Similarly, in Fig. 14(c), the red curve has a fifth turning point

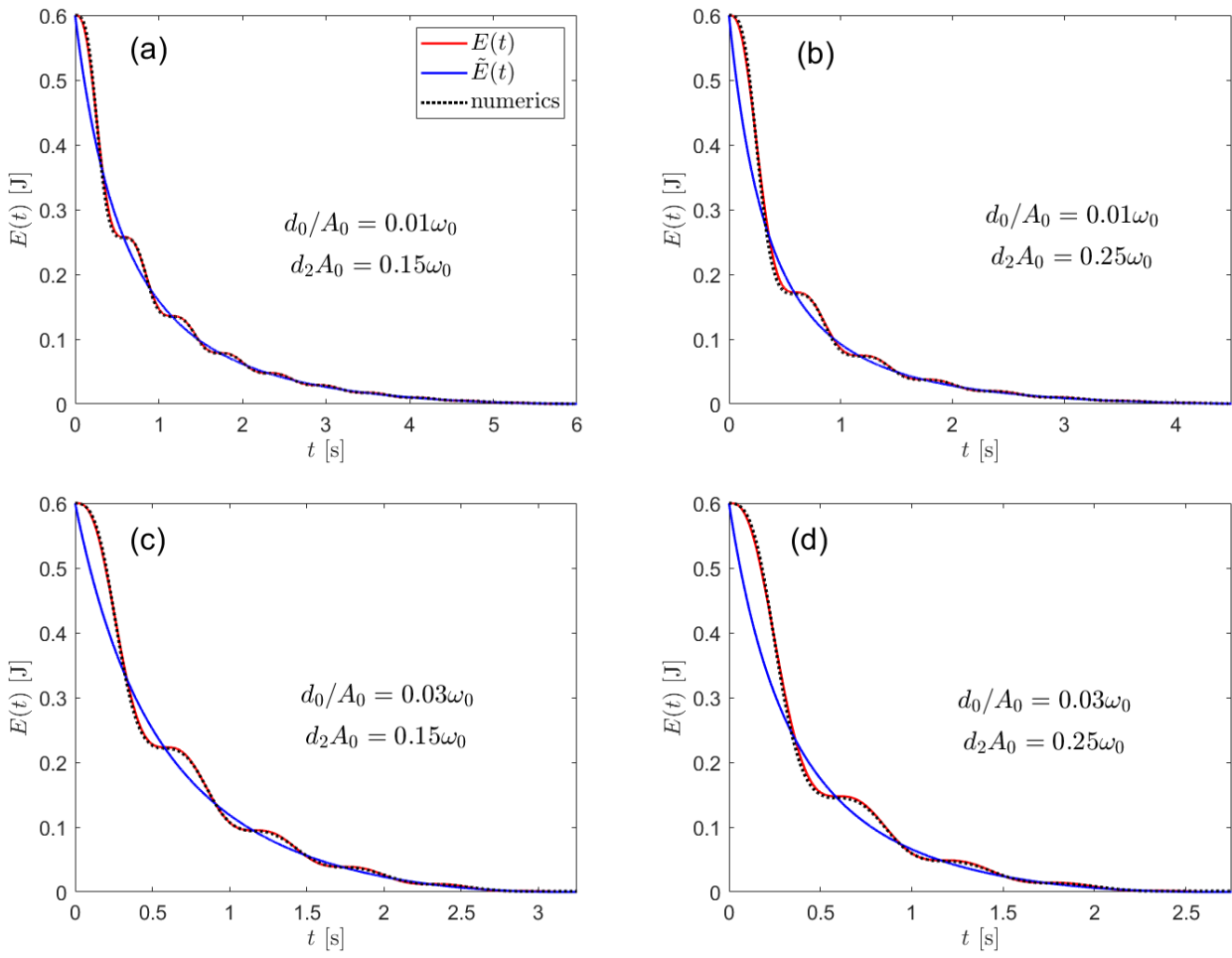


FIG. 15: Energies corresponding to solutions shown in Fig. 14(a)-(d). See text for details.

with a displacement just slightly less in magnitude than  $\mu mg/k$ , thus the fourth turning point of the solid red curve shown in Fig. 14(c) is the last turning point with a displacement greater in magnitude than  $\mu mg/k$ . In any case, although, depending on the range shown, it may not be easy to visually determine which of the turning points is the last turning point with the displacement greater in magnitude than  $\mu mg/k$ , this can certainly be easily done in various ways, e.g., simply by zooming in on the area of interest on the graph and reading out the coordinates of the required turning point or by using available functions in software packages, such as MATLAB, to filter these coordinates from the numerical data provided by the expression (47). Thus, for any choice of initial conditions and values  $d_0$  and  $d_2$ , the coordinates  $(t_0, x(t_0))$  can be easily determined.

From the results shown in Section III, it is clear that the damping quadratic in velocity has the highest influence on the dynamics within the first few half-periods. Thus, in the case of combined quadratic and Coulomb damping, towards the very end of the dynamics, we expect Coulomb damping to dominate. Therefore, the dynamics for  $t > t_0$  can be well described even if we completely ignore the contribution of the quadratic damping, i.e. if we take that the exact solution of equation of motion (3) with purely Coulomb damping, with initial conditions  $(x(t_0) \neq 0, v(t_0) = 0)$ , describes the dynamics for  $t > t_0$ . In that case, we obtain

$$x(t) = \begin{cases} A f(t) \cos(\omega_0 t + \varphi) & \text{if } 0 \leq t \leq t_0 \\ (x(t_0) - \text{sgn}[x(t_0)] \frac{\mu mg}{k}) \cos(\omega_0(t - t_0)) + \text{sgn}[x(t_0)] \frac{\mu mg}{k} & \text{if } t_0 < t \leq t_0 + \pi/\omega_0 \\ -x(t_0) + 2 \text{sgn}[x(t_0)] \frac{\mu mg}{k} & \text{if } t > t_0 + \pi/\omega_0 \end{cases} \quad (52)$$

as an improved approximate analytical solution, where  $f(t)$  is given by (45), and

$$v(t) = \begin{cases} -\omega_0 A f(t) \sin(\omega_0 t + \varphi) + A \frac{df(t)}{dt} \cos(\omega_0 t + \varphi) & \text{if } 0 \leq t \leq t_0 \\ -\omega_0 (x(t_0) - \text{sgn}[x(t_0)] \frac{\mu mg}{k}) \sin(\omega_0(t - t_0)) & \text{if } t_0 < t \leq t_0 + \pi/\omega_0 \\ 0 & \text{if } t > t_0 + \pi/\omega_0 \end{cases} \quad (53)$$

as the corresponding velocity. In Fig. 16(a) and (b) we show improved solutions  $x(t)$  given by (52), solutions  $\tilde{x}(t)$  given by (49) and the corresponding numerical solutions for the same initial conditions and ratios  $d_0/(\omega_0 A_0)$  and  $d_2 A_0/\omega_0$  as used in Fig. 14(c) and (d). We see that solution (52) gives an excellent approximation of the instant and the position of the halt. In Fig. 17(a) and (b) we show the energy  $E(t) = kx(t)^2/2 + mv(t)^2/2$  obtained using (52)

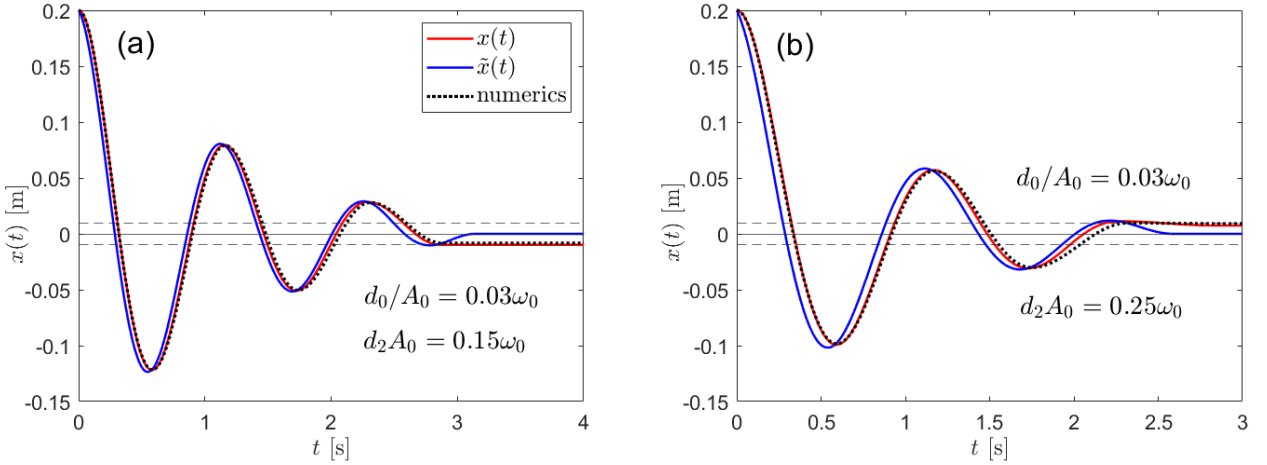


FIG. 16: Solid red curves show the improved solutions  $x(t)$  given by (52), with initial conditions  $(x_0 = 0.2m, v_0 = 0)$  for  $d_0/(\omega_0 A_0) = 0.03$  and  $d_2 A_0/\omega_0 = \{0.15, 0.25\}$ . Solid blue curves show the solutions  $\tilde{x}(t)$  given by (49) and black dotted curves show the numerical solutions for the same initial conditions and the corresponding values of the ratios  $d_0/(\omega_0 A_0)$  and  $d_2 A_0/\omega_0$ . The dashed horizontal lines in each figure are positioned at corresponding  $\pm \mu mg/k$  values, i.e. they indicate the region within which  $|x(t)| \leq \mu mg/k$  holds. See text for details.

and (53), the energy  $\tilde{E}(t)$  corresponding to the solution (49), and the numerically obtained energies for the same initial conditions and ratios  $d_0/(\omega_0 A_0)$  and  $d_2 A_0/\omega_0$  as used in Fig. 16(a) and (b). We can see that the energies  $E(t)$ , obtained with (52) and (53), agree excellently with the numerically obtained energies, as expected, since, in the context of energy alone, even the less precise approximate solution (47), and the corresponding velocity (48), resulted in excellent approximation of numerically obtained energies.

However, if, e.g., we are not satisfied with the precision with which the solution (52) describes the dynamics, we will show how it can be further improved. In the example of the solution (47) shown in Fig. 14(d), the fourth turning point  $(t_0, x(t_0))$ , marked by a red arrow, has a displacement  $x(t_0)$  only slightly greater than  $\mu mg/k$ , so the corresponding improved solution, i.e. (52), necessarily halts before reaching the equilibrium position, i.e. the last zero crossing occurred before the instant  $t_0$ , and therefore the improved solution (52), shown in Fig. 16(b), does not make any correction to the instant of the last zero crossing. In Fig. 14(d), the green arrow points to the third turning point of the solution (47), with the coordinates  $(t_3, x(t_3)) = (1.74s, -0.155x_0)$ , where we used subscript 3 simply to denote the third turning point. If we ignore the quadratic damping for  $t > t_3$ , we can take

$$x(t) = \begin{cases} Af(t) \cos(\omega_0 t + \varphi) & \text{if } 0 \leq t \leq t_3 \\ (x(t_3) + \frac{\mu mg}{k}) \cos(\omega_0(t - t_0)) - \frac{\mu mg}{k} & \text{if } t_3 < t \leq t_3 + \pi/\omega_0 \\ (x(t_3) + 3\frac{\mu mg}{k}) \cos(\omega_0(t - t_0)) + \frac{\mu mg}{k} & \text{if } t_3 + \pi/\omega_0 < t \leq t_3 + 2\pi/\omega_0 \\ x(t_3) + 4\frac{\mu mg}{k} & \text{if } t > t_3 + 2\pi/\omega_0 \end{cases} \quad (54)$$

as an further improved approximate solution, where again  $f(t)$  is given by (45). We note here that (54) is derived for the specific example with  $x(t_3) < 0$ , and it is easy to derive expressions that apply to the case with opposite sign. In Fig. 18 we show the solution (54) and we can see a better overall agreement with the numerical solution compared to the solution (52) shown in Fig. 16(b). Therefore, in the cases when the last turning point with a displacement

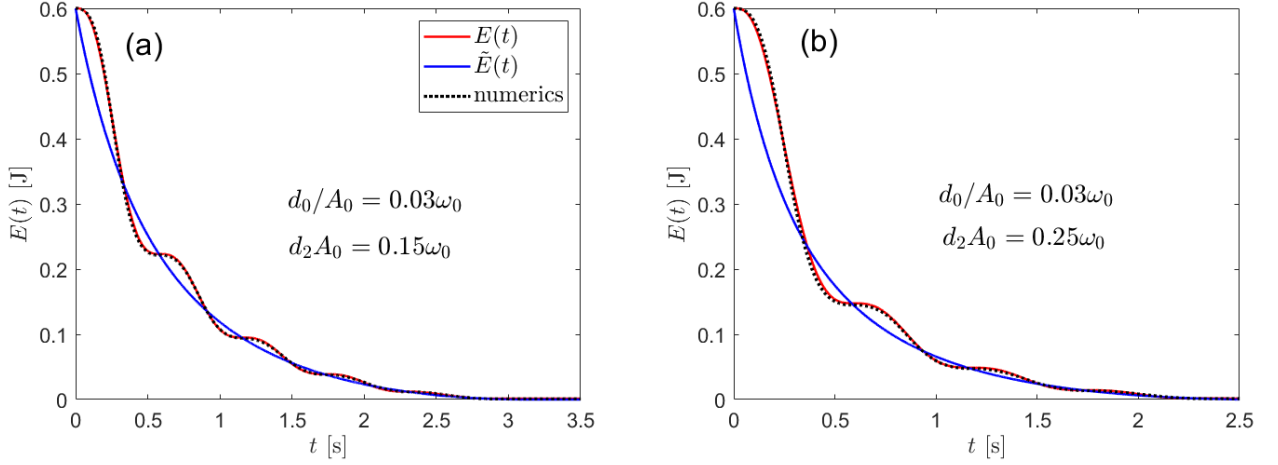


FIG. 17: Solid red curves show the energies  $E(t)$ , obtained using (52) and (53), for the same initial conditions and values of the ratios  $d_0/(\omega_0 A_0)$  and  $d_2 A_0/\omega_0$  as used in Fig. 16(a) and (b). Solid blue curves show the energies  $\tilde{E}(t)$  corresponding to solutions (49), and black dotted curves show the numerically obtained energies, both for the same initial conditions and values of the ratios as used for  $E(t)$ . See text for details.

greater in magnitude than  $\mu mg/k$ , i.e.  $(t_0, x(t_0))$ , has only slightly greater displacement than  $\mu mg/k$ , i.e. when  $|x(t_0)| \gtrsim \mu mg/k$ , we can take the coordinates of the turning point that precedes it, calculate the exact solution of equation of motion (3) with purely Coulomb damping starting from that instant, and get a better overall description of the dynamics.

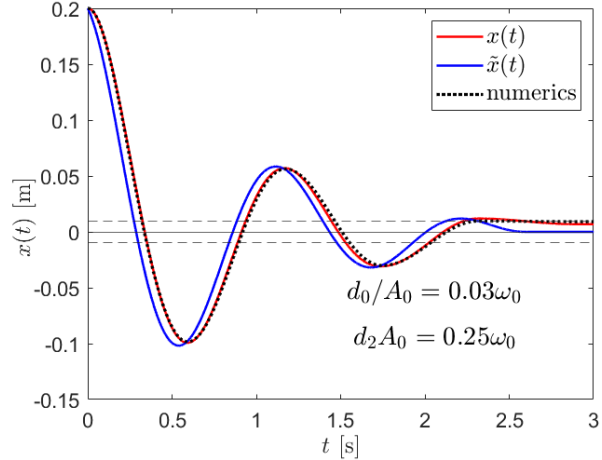


FIG. 18: Solid red curve shows the solution  $x(t)$  given by (54), with initial conditions  $(x_0 = 0.2m, v_0 = 0)$  for  $d_0/(\omega_0 A_0) = 0.03$  and  $d_2 A_0/\omega_0 = 0.25$ . Solid blue curve shows the solution  $\tilde{x}(t)$  given by (49) and black dotted curve shows the numerical solution for the same initial conditions and the same values of the ratios  $d_0/(\omega_0 A_0)$  and  $d_2 A_0/\omega_0$ . The dashed horizontal lines are positioned at corresponding  $\pm \mu mg/k$  values, i.e. they indicate the region within which  $|x(t)| \leq \mu mg/k$  holds. See text for details.

### B. Initial conditions ( $x_0 = 0, v_0 > 0$ )

For this type of initial conditions, equation (43) simplifies to  $A = A_0 = v_0/\omega_0$  and we get  $\varphi = \varphi_0 = -\pi/2$ , i.e. (47) and (49) become equal. The improved solution, i.e. (52), is, of course, also valid for these initial conditions, it

is only necessary to determine the values  $(t_0, x(t_0))$  of the last turning point of the function  $Af(t) \cos(\omega_0 t + \varphi)$  with property  $|x(t_0)| > \mu mg/k$ , and insert these values into expression (52). As an example of the dynamics with these type of initial conditions, in Fig. 19(a) we show the solutions (52), (49) and the corresponding numerical solutions for  $d_0/(\omega_0 A_0) = 0.03$  and  $d_2 A_0 / \omega_0 = 0.25$ . In this case,  $(t_0, x(t_0))$  is the fourth turning point, solutions (52) and (49) overlap for  $0 < t \leq t_0$ , and for  $t > t_0$  the solution (52) agrees significantly better with the numerical solution compared to (49). In Fig. 19(b) we show the energies corresponding to solutions shown in Fig. 19(a).

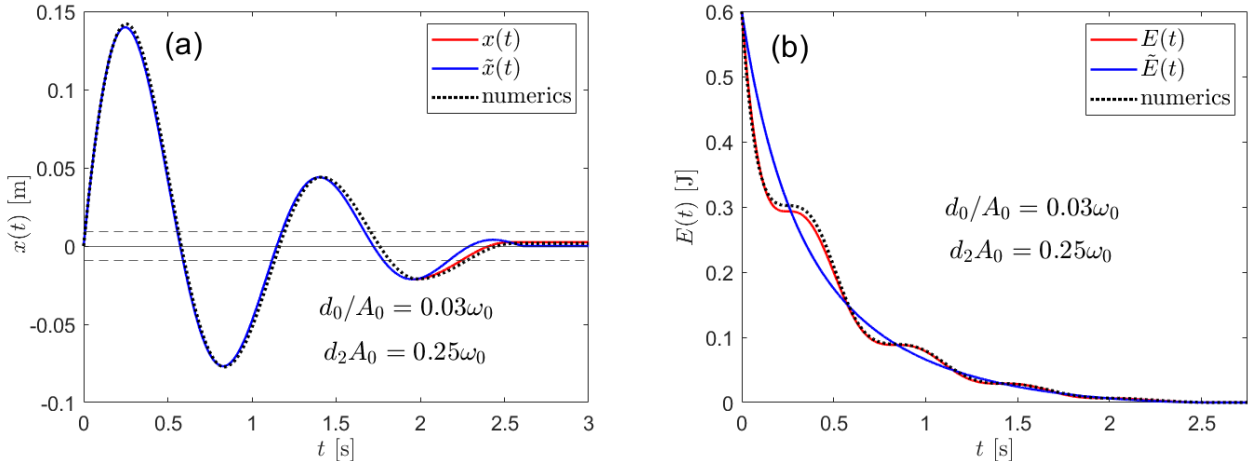


FIG. 19: (a) Solid red curves show the solution (52) with initial conditions  $(x_0 = 0, v_0 = \omega_0 A_0)$ ,  $d_0/(\omega_0 A_0) = 0.03$  and  $d_2 A_0 / \omega_0 = 0.25$ . Solid blue curves show the corresponding solution (49) and black dotted curves show the corresponding numerical solution. The dashed horizontal lines are positioned at  $\pm \mu mg/k$ , i.e. they indicate the region within which  $|x(t)| \leq \mu mg/k$  holds. (b) The energies corresponding to solutions shown in figure (a). See text for details.

### C. Initial conditions $(x_0 \neq 0, v_0 \neq 0)$

As an example, here we choose  $(x_0 = A_0 \sqrt{2}/2, v_0 = \omega_0 x_0)$ ,  $d_0/(\omega_0 A_0) = 0.03$  and  $d_2 A_0 / \omega_0 = 0.25$ . For this type of initial conditions, equation (43) remains a quartic equation in  $A$ . Again, instead of delving into solving the corresponding quartic equation analytically, we solve it using the *roots* MATLAB function. Of the four solutions we obtained, the closest to the value  $A_0 = 0.2m$  is  $A = 0.234m$ , which corresponds to the initial phase  $\varphi = -0.922$ . In Fig. 20(a) we show the solutions (52), (49) and the numerical solutions corresponding to this choice of the initial conditions and values of the ratios  $d_0/(\omega_0 A_0)$  and  $d_2 A_0 / \omega_0$ . In this case,  $(t_0, x(t_0))$  used in the solution (52) is the fifth turning point. In Fig. 20(b) we show the energies corresponding to the solutions shown in Fig. 20(a).

Since the displacement of the fifth turning point of the solid red curve, shown in Fig. 20(a), is only slightly greater in magnitude than  $\mu mg/k$ , we will also consider the solution which we obtain if we completely ignore the quadratic damping from the instant of the fourth turning point  $(t_4, x(t_4))$  onward, i.e. for  $t > t_4$ . Thus, we can use again the solution of the form (54), but with  $(t_4, x(t_4)) = (1.84s, -0.146x_0)$  in place of  $(t_3, x(t_3))$ , and with the values of  $A$  and  $\varphi$  corresponding to initial conditions used here. The results are shown in Fig. 21. Again, similarly as in Fig. 18, we see that we can completely ignore the quadratic damping in the last two half-periods and still get a good description of the dynamics.

### D. Comments on results for harmonic oscillator with combined quadratic and Coulomb damping

The results presented in this section show that the new approximate analytical solutions (47) with the corresponding  $A$  and  $\varphi$ , provide a significantly better description of the dynamics compared to the solutions (49) which are provided by the approach used in [14]. For the range of damping constants  $\mu$  and  $D$  such that  $0 < d_0/(\omega_0 A_0) \leq 0.03$  and  $0 < d_2 A_0 / \omega_0 \leq 0.25$  hold, solutions (47) provide a good description of the dynamics for all types of initial conditions, unless we are concerned with high precision of the description at the very end of the dynamics, e.g. for the last half-period or last two half-periods before the halt.

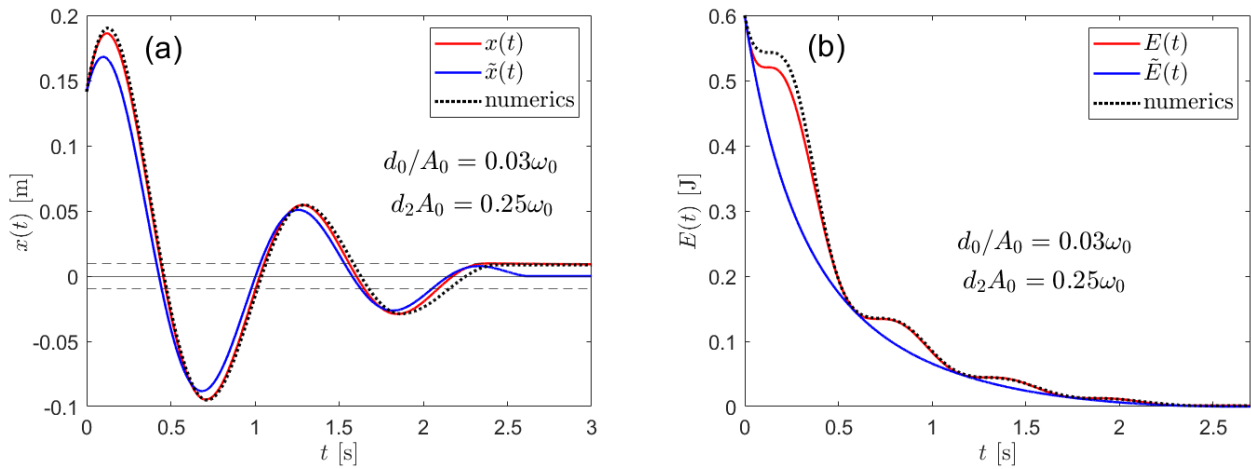


FIG. 20: (a) Solid red curves show the solution (52) with initial conditions  $(x_0 = A_0\sqrt{2}/2, v_0 = \omega_0 x_0)$ , for  $d_0/(A_0\omega_0) = 0.03$  and  $d_2 A_0/\omega_0 = 0.25$ . Solid blue curves show the corresponding solution (49) and black dotted curves show the corresponding numerical solution. The dashed horizontal lines are positioned at  $\pm \mu mg/k$ , i.e. they indicate the region within which  $|x(t)| \leq \mu mg/k$  holds. (b) The energies corresponding to solutions shown in figure (a). See text for details.

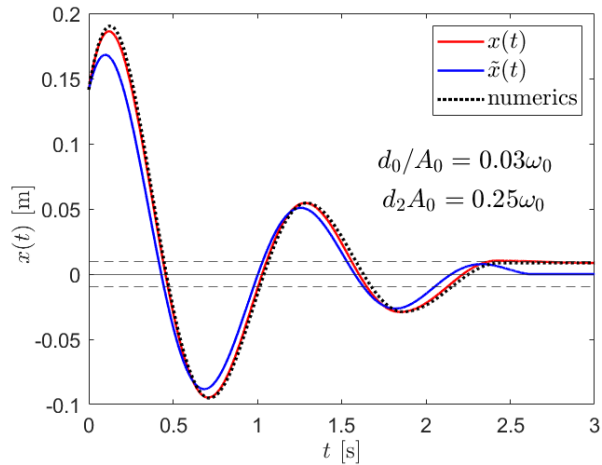


FIG. 21: Solid red curve shows the solution  $x(t)$  of the form (54), but with  $(t_4, x(t_4)) = (1.84s, -0.146x_0)$  in place of  $(t_3, x(t_3))$ , with initial conditions  $(x_0 = A_0\sqrt{2}/2, v_0 = \omega_0 x_0)$  for  $d_0/(A_0\omega_0) = 0.03$  and  $d_2 A_0/\omega_0 = 0.25$ . Solid blue curve shows the solution  $\tilde{x}(t)$  given by (49) and black dotted curve shows the numerical solution for the same initial conditions and the same values of the ratios  $d_0/(\omega_0 A_0)$  and  $d_2 A_0/\omega_0$ . The dashed horizontal lines are positioned at corresponding  $\pm \mu mg/k$  values, i.e. they indicate the region within which  $|x(t)| \leq \mu mg/k$  holds. See text for details.

In case we need greater precision in the description of the last or the last two half-periods before the halt, we introduced solutions (52) and (54), which significantly correct the limitations of solution (47). The trick was to exploit the physics of the problem, i.e. to completely ignore the influence of damping quadratic in velocity during the last or last two half-periods of the motion, due to small velocity during these time intervals, and take that only Coulomb damping decreases the oscillations towards the end of the dynamics.

In Fig. 14(d), we can see, in the case  $d_0/(\omega_0 A_0) = 0.03$  and  $d_2 A_0/\omega_0 = 0.25$ , that the amplitude of the solid red curve after the first period drops to about 30% of the initial value. Thus, the new approximate analytical solutions, introduced in this section, describe the dynamics well for damping that we could characterize (at least) as moderately strong.

## VI. CONCLUSION AND OUTLOOK

By comparing our new analytical solutions with numerical solutions, we have shown that they provide an excellent description of the dynamics of a harmonic oscillator damped by a force quadratic in velocity, sliding friction, and by the combination of these two damping forces. Our approach is valid for any type of initial conditions and for a wide range of values of the damping constants, which makes it suitable for the description and analysis of free damped vibrations of single-degree-of-freedom systems in the context of experiments in physics and engineering applications. The most elegant result is obtained for the damping quadratic in velocity analyzed in Section III. In that case, the initial amplitude  $A$  is easily obtained analytically for any type of initial conditions by solving a simple quadratic equation. In the remaining two cases, depending on the type of initial conditions, it is necessary to solve the quartic equation to obtain initial amplitude  $A$ , which is not easy to do analytically, but can be very easily solved numerically with standard and accessible software packages. Once we have determined  $A$ , the initial phase  $\varphi$  is easy to calculate in any case.

Equation (22) suggests that the important combination of damping linear in velocity and damping quadratic in velocity will also be easily handled by our approach, since in that case (22) becomes a quadratic equation and the initial amplitude  $A$  can be easily determined analytically for any type of initial conditions. This case is particularly important because in order to fully model the influence of air resistance, both types of damping are needed [11, 13, 15, 20]. Furthermore, we can expect that the approach presented in this paper will bring significant improvements in the description of the dynamics compared to the solutions already obtained in [14] for this combination of damping forces, because both damping linear in velocity and damping quadratic in velocity contribute to a significant change in the initial phase compared to the initial phase of the undamped case. Finally, the dynamics of every real-world system is also, to a greater or lesser extent, influenced by a force of sliding friction. Therefore, for a full description of the damping of free vibrations in real-world systems, it is necessary to take into account that all three types of damping are active, and how much each of them affects the dynamics depends, of course, on the specifics of the particular system we are considering, but also on the initial conditions (due to the nonlinear terms in the corresponding equation of motion). We will analyze in detail the new approximate analytical solutions for all remaining combinations of the three types of damping in a follow-up paper (i.e. in Part II).

## VII. ACKNOWLEDGMENTS

K.L. and R.P. acknowledge support from the project “Implementation of cutting-edge research and its application as part of the Scientific Center of Excellence for Quantum and Complex Systems, and Representations of Lie Algebras”, Grant No. PK.1.1.10.0004, co-financed by the European Union through the European Regional Development Fund - Competitiveness and Cohesion Programme 2021-2027.

---

[1] Frank S. Crawford. *Waves: Berkeley Physics Course. volume 3*. McGraw-Hill, New York, 1968.

[2] J.D. Cutnell and K.W. Johnson. *Physics*. John Wiley & Sons, 2009.

[3] David Halliday, Robert Resnick, and Jearl Walker. *Fundamentals of Physics*. John Wiley & Sons, 2013.

[4] Hugh D. Young and Roger A. Freedman. *University Physics with Modern Physics*. Pearson, 2020.

[5] I. R. Lapidus. Motion of a harmonic oscillator with sliding friction. *American Journal of Physics*, 38(11):1360–1361, nov 1970.

[6] A. Marchewka, David. S. Abbott, and R. J. BeichnerKamela. Oscillator damped by a constant-magnitude friction force. *American Journal of Physics*, 72(4):477–483, apr 2004.

[7] A. Anastasios Adamopoulos and N. Adamopoulos. Constant and quadratic damping of free oscillations: easy solutions. *International Journal of Mathematical Education in Science and Technology*, 53(11):3151–3161, jan 2022.

[8] M. Kamela. An oscillating system with sliding friction. *The Physics Teacher*, 45(2):110–113, feb 2007.

[9] B. R. Jr. Smith. The quadratically damped oscillator: A case study of a non-linear equation of motion. *American Journal of Physics*, 80(9), sep 2012.

[10] C. E. Mungan and T. C. Lipscombe. Oscillations of a quadratically damped pendulum. *European Journal of Physics*, 34(5):1243–1253, jul 2013.

[11] X. Wang, C. Schmitt, and M. Payne. Oscillations with three damping effects. *European Journal of Physics*, 23(2):155–164, jan 2002.

[12] Karlo Lelas, Nikola Poljak, and Dario Jukić. Damped harmonic oscillator revisited: The fastest route to equilibrium. *American Journal of Physics*, 91(10):767–775, 10 2023.

[13] P. T. Squire. Pendulum damping. *American Journal of Physics*, 54(11):984–991, nov 1986.

- [14] K. Lelas and R. Pezer. The amplitude decay of a harmonic oscillator damped simultaneously by weak linear and nonlinear damping forces. *European Journal of Physics*, 46(4):045001, jun 2025.
- [15] R. A. Nelson and M. G. Olsson. The pendulum—rich physics from a simple system. *American Journal of Physics*, 54(2):112–121, feb 1986.
- [16] M. V. Vitorino, A. Vieira, and M. S. Rodrigues. Effect of sliding friction in harmonic oscillators. *Scientific Reports*, 7:3726, jun 2017.
- [17] K. Lelas and R. Pezer. Modeling the amplitude and energy decay of a weakly damped harmonic oscillator using the energy dissipation rate and a simple trick. *European Journal of Physics*, 46(1):015004, dec 2024.
- [18] P. F. Hinrichsen and C. I. Larnder. Combined viscous and dry friction damping of oscillatory motion. *American Journal of Physics*, 86(8):577–584, aug 2018.
- [19] B. K. Karthik, R. B. Shreesha, V. Shrikanth, and A. K. Gaonkar. Prediction of energy dissipation by analytical solution to combined viscous and coulomb damping. *Journal of Sound and Vibration*, 573:118216, 2024.
- [20] M. E. Bacon and D. D. Nguyen. Real-world damping of a physical pendulum. *European Journal of Physics*, 26(4):651–655, may 2005.
- [21] L. Cveticanin. Oscillator with strong quadratic damping force. *Publications de l’Institut Mathématique (Beograd)*, 85(99):119–130, 2009.
- [22] L. Cveticanin. Oscillators with nonlinear elastic and damping forces. *Computers & Mathematics with Applications*, 62(4):1745–1757, aug 2011.
- [23] J. A. Rizcallah. Revisiting the coulomb-damped harmonic oscillator. *European Journal of Physics*, 40(5), aug 2019.